

Enhanced sensitivity to variations of fundamental constants in highly charged molecules from analytic perturbation theory

Carsten Zülch,¹ Konstantin Gaul,¹ and Robert Berger^{1,*}

¹*Fachbereich Chemie, Philipps-Universität Marburg, Hans-Meerwein-Straße 4, 35032 Marburg*

(Dated: November 17, 2025)

Quasi-forbidden electronic transitions in atoms and quasi-degenerate vibronic transitions in molecules serve as powerful probes of hypothetical temporal variations of fundamental constants. Computation of the sensitivity of a transition to a variation of the fine-structure constant is conventionally performed by numerical variation of the speed of light in sophisticated electronic structure calculations, and therewith several individual calculations have to be performed. An approach is presented herein that obtains sensitivity coefficients as first order perturbation to the Dirac-Coulomb Hamiltonian and allows their computation as expectation values of the relativistic kinetic energy and rest-mass operators. These are available in essentially all *ab initio* relativistic electronic structure codes. Additionally, the corresponding operators for two-component Hamiltonians are derived, explicitly for the zeroth order regular approximation Hamiltonian. The approach is applied to demonstrate great sensitivity of highly charged polar molecules that were recently proposed for high-precision spectroscopy in [Zülch *et al.*, arXiv:2203.10333[physics.chem-ph]]. In particular, a high sensitivity of a wealth of quasi-degenerate vibronic transitions in PaF³⁺ and CeF²⁺ to temporal variations of the fine-structure constant and the electron-proton mass ratio is shown.

I. INTRODUCTION

Theories unifying gravity and quantum mechanics predict temporal variations of fundamental constants (VFC), such as the fine-structure constant α and the electron-proton mass-ratio $\mu = m_e/m_p$, with the expansion of our universe (see Review [1]). Moreover, such variations could arise from dependence of α and μ on the gravitational potential and can be a signature of scalar bosonic dark matter like dilatons. Precision spectroscopy of atoms and molecules gave one of the most stringent limits of the variations of α and μ [1]. The so far best upper bound on a temporal variation of these two dimensionless quantities was obtained by comparing two transition frequencies in Yb⁺ [2–4]: $\delta\mu/\mu < 10^{-17}$ yr and $\delta\alpha/\alpha < 10^{-18}$ yr, where a 10-fold improvement is expected in near future [5]. Heavy-element-containing diatomic molecular ions [6–11] and highly charged atoms are promising candidates for improvement of these bounds as per their much higher sensitivity due to strong relativistic effects and transitions that have very small linewidths [12, 13].

For identifying transitions that appear favourable for detecting VFC, atomic and molecular theory is required. To the best of our knowledge, in all previous theoretical studies of VFC, the electronic enhancement of an α variation was determined by numerically varying the speed of light in relativistic electronic structure calculations. This requires to perform an array of possibly quite demanding computations to obtain the sensitivity to temporal variations of α .

This tedious numerical procedure for obtaining enhancement factors, which becomes particular costly for

larger molecular systems or for high-level many-body approaches, can likely be considered as one of the reasons for the relatively low number of (*ab initio*) predictions presently available. Predictions for atomic systems are somewhat more abundant (see e. g. [5, 14]), whereas for molecular systems information is scarce [6, 11, 15, 16] (see also Ref. [17] and [18], as well as references therein).

In this paper we show that within relativistic four-component approaches, the sensitivity to a small variation of the fine-structure constant can be calculated directly as expectation value of the Dirac kinetic energy and electronic rest-mass operators scaled by a constant factor. We demonstrate the applicability for four-component and quasi-relativistic two-component calculations, discuss higher-order effects and demonstrate the consistency by comparison to the Pauli expansion. The method proposed is directly amenable to common relativistic electronic structure programs such as Dirac [19] as the perturbing operators needed are already available.

We utilise this analytic approach to compute the VFC sensitivity of stable polar highly charged molecular ions such as PaF³⁺, which we recently suggested as prospective laboratories for precision tests of fundamental physics [20]. Such systems possess close-lying electronic states of different symmetry and exhibit large relativistic effects. Thus, we anticipated them to be ideal candidates to search for VFC [20, 21]. Furthermore, we study CeF²⁺ alongside PaF³⁺, as both ions feature similar electronic characteristics for the lower electronic states. We demonstrate a high sensitivity of both highly charged species to variations of α and μ by application of our novel approach.

* robert.berger@uni-marburg.de

II. THEORY

A. Influence of variations of α and μ on vibronic transition frequencies

Assuming that the fine-structure constant α varies by a small amount $\delta\alpha$ we can define the red-shifted fine-structure constant α_z as $\alpha_z = \alpha + \delta\alpha$. In leading order, the electronic transition wavenumber in an atom or molecule changes with the red-shifted fine structure constant as [14, 22]

$$\tilde{\nu} = \tilde{\nu}_{\text{el}} + \Delta q_1 \left(\left(\frac{\alpha_z}{\alpha} \right)^2 - 1 \right) + \Delta q_2' \left(\left(\frac{\alpha_z}{\alpha} \right)^4 - 1 \right) + \mathcal{O}(\alpha_z^6). \quad (1)$$

Here q_1 and q_2' describe the sensitivity to a variation of the fine-structure constant and need to be determined from electronic structure theory. As $\delta\alpha$ is expected to be as small as $\delta\alpha/\alpha \lesssim 10^{-18}$ [4] for practical purposes only q_1 will be relevant. We will use a slight modification of the definition of q_2' and write (now with q_2 instead of q_2')

$$\tilde{\nu} = \tilde{\nu}_{\text{el}} + \Delta q_1 \tilde{x} + \Delta q_2 \tilde{x}^2 + \mathcal{O}(\tilde{x}^3). \quad (2)$$

where we used the variable

$$\tilde{x} = \left(\frac{\alpha + \delta\alpha}{\alpha} \right)^2 - 1 = \frac{2\delta\alpha}{\alpha} + \frac{\delta\alpha^2}{\alpha^2}. \quad (3)$$

This formulation, which was also chosen in Ref. [23], is consistent with the overall α -dependence in relativistic electronic structure theory and coincides with the Pauli expansion as we demonstrate later.

A change, $\delta\tilde{\nu}_v$, in the vibronic transition wavenumber $\tilde{\nu}_v$ of a molecule, where the subscript v indicates the vibrational transition, due to a temporal variation $\delta\alpha$ of α , and $\delta\mu$ of μ reads in leading order[6] as

$$\delta\tilde{\nu}_v = \Delta q_1 \tilde{x} - \frac{\tilde{\nu}_{\text{vib}}}{2} \frac{\delta\mu}{\mu}, \quad (4)$$

where $\tilde{x} \sim 2\delta\alpha/\alpha$ and $\tilde{\nu}_{\text{vib}}$ is the pure vibrational transition wavenumber for transition v . Note that we utilised here the harmonic approximation for the vibrational contribution.

The overall enhancements $K_{\alpha,v}$, $K_{\mu,v}$ of variations of fundamental constants α and μ is found from the leading-order dependence of the transition wavenumber $\tilde{\nu}_v$ on the fundamental constants [6]

$$\frac{\delta\tilde{\nu}_v}{\tilde{\nu}_v} \approx \frac{2\Delta q_1}{\tilde{\nu}_v} \frac{\delta\alpha}{\alpha} - \frac{\tilde{\nu}_{\text{vib}}}{2\tilde{\nu}_v} \frac{\delta\mu}{\mu} = \left(K_{\alpha,v} \frac{\delta\alpha}{\alpha} + K_{\mu,v} \frac{\delta\mu}{\mu} \right). \quad (5)$$

B. Variation of α as small perturbation to the Dirac-Coulomb Hamiltonian

We start from the Dirac-Coulomb (DC) Hamiltonian in which the potential energy operator is α independent.

Additional relativistic corrections to the potential energy of order α^2 , such as those caused by the Breit interaction, can become relevant in particular for light elements but are expected to be negligible for heavy-elemental systems such as CeF^{2+} and PaF^{2+} . When quadratic effects (q_2) are desired, leading order quantum electrodynamics (QED) corrections could contribute to these as well (see Ref. [24] for our recent approaches to incorporate QED corrections within a two-component framework), but those are neglected in our present work.

The electronic one-particle DC-Hamiltonian reads

$$\hat{H}_{\text{DC}} = c\vec{\alpha} \cdot \hat{p} + (\beta - \mathbf{1}) m_e c^2 + \hat{V}_C, \quad (6)$$

where we shifted the energy spectrum by $m_e c^2$, with c being the speed of light, and used the one-electron linear momentum operator $\hat{p} = -i\hbar\vec{\nabla}$, the instantaneous Coulomb interaction \hat{V}_C , the standard Dirac matrices $\vec{\alpha}$, β and the 4×4 unit matrix $\mathbf{1}$. In atomic units, m_e has the numerical value of 1 and c the numerical value of α^{-1} yielding

$$\hat{H}_{\text{DC}} = \alpha^{-1} \vec{\alpha} \cdot \hat{p} + (\beta - \mathbf{1}) \alpha^{-2} + \hat{V}_C. \quad (7)$$

As mentioned above, possible variations $\delta\alpha$ in the fine structure constant are expected to be on the order $\delta\alpha/\alpha \lesssim 10^{-18}$ allowing the use of first order perturbation theory. For such a small variation in α we set $\alpha \rightarrow \alpha + \delta\alpha$ yielding the perturbed DC-Hamiltonian

$$\hat{H}_{\text{DC}} = \frac{1}{\alpha + \delta\alpha} \vec{\alpha} \cdot \hat{p} + (\beta - \mathbf{1}) \frac{1}{(\alpha + \delta\alpha)^2} + \hat{V}_C. \quad (8)$$

To find the leading order perturbations in $\delta\alpha$ for the DC-Hamiltonian, we use following expansion employing the definition (3):

$$\begin{aligned} \frac{1}{\alpha + \delta\alpha} &= \alpha^{-1} \frac{1}{1 + \delta\alpha/\alpha} = \alpha^{-1} \frac{1}{\sqrt{1 + \tilde{x}}} \\ &= \alpha^{-1} \sum_{k=0}^{\infty} \left[\frac{(2k)!}{(k!)^2} \left(-\frac{\tilde{x}}{4} \right)^k \right] \end{aligned} \quad (9)$$

$$\frac{1}{(\alpha + \delta\alpha)^2} = \alpha^{-2} \frac{1}{1 + \tilde{x}} = \alpha^{-2} \sum_{k=0}^{\infty} [-\tilde{x}]^k, \quad (10)$$

Under a variation in the fine-structure constant the DC-Hamiltonian, thus, takes the form

$$\begin{aligned} \hat{H}_{\text{DC}} &= \underbrace{c\vec{\alpha} \cdot \hat{p} + \hat{V}_C}_{\hat{H}_{\text{DC}}} + (\beta - \mathbf{1}) c^2 \\ &+ \underbrace{\sum_{k=1}^{\infty} \left[(-\tilde{x})^k \left(\frac{(2k)!}{(k!)^2 4^k} c\vec{\alpha} \cdot \hat{p} + (\beta - \mathbf{1}) c^2 \right) \right]}_{\hat{H}_{\text{DC}}(\delta\alpha)} \end{aligned} \quad (11)$$

As $\delta\alpha$ is very small, first order perturbation theory is sufficient for practical purposes and we obtain the perturbing operator

$$\hat{H}_{\text{DC}}^{(1)} = \left. \frac{\partial \hat{H}_{\text{DC}}(\delta\alpha)}{\partial \tilde{x}} \right|_{\delta\alpha=0} = -\frac{c}{2} \vec{\alpha} \cdot \hat{p} - (\beta - \mathbf{1}) c^2 \quad (12)$$

This operator is just the sum of the rest-mass and kinetic energy operators of the DC-Hamiltonian with a different prefactor, which are available in essentially any relativistic quantum chemistry program package. Thus, it is straightforward to obtain q_1 as the expectation value (with hc_0 as a conversion factor from wavenumber units to energy units)

$$hc_0q_1 = \left\langle \hat{H}_{\text{DC}}^{(1)} \right\rangle. \quad (13)$$

If there is a need to know q_2 , it can be obtained within second order perturbation theory as

$$hc_0q_2 = \left\langle \hat{H}_{\text{DC}}^{(2)} \right\rangle + \sum_{i \neq 0} \frac{\left| \left\langle \Psi_0 \left| \hat{H}_{\text{DC}}^{(1)} \right| \Psi_i \right\rangle \right|^2}{E_0 - E_i}, \quad (14)$$

where we have used for notational brevity a sum-over-states formulation. The sum runs over electronic states i , except 0, of energies E_i with wave functions Ψ_i , whereas Ψ_0 and E_0 denote the wave function and energy of the targeted reference state. The second order Hamiltonian is

$$\hat{H}_{\text{DC}}^{(2)} = \left. \frac{\partial^2 \hat{H}_{\text{DC}}(\delta\alpha)}{\partial \tilde{x}^2} \right|_{\delta\alpha=0} = \frac{3}{4} c \tilde{\alpha} \cdot \hat{p} + 2(\beta - 1) c^2, \quad (15)$$

which also contains only rest-mass and kinetic energy operators with a different weighting.

C. Quasi-relativistic Hamiltonians

In a quasi-relativistic theory the small component $\psi_{\text{D}}^{\text{S}}$ of the DC bi-spinor is not treated explicitly but can be computed in good approximation from the one-particle two-component wave function as $\psi_{\text{D}}^{\text{S}} \approx \psi_{2c}^{\text{S}} = c(2c^2\mathbf{1} + E\mathbf{1} - \mathcal{V})^{-1} \tilde{\sigma} \cdot \hat{p} \psi_{2c}^{\text{L}}$, where we assume no external fields. We introduced the general non-diagonal two-component potential \mathcal{V} to accommodate a common formalism before giving explicit expressions for different flavours of quasi-relativistic methods below. The approximate methods differ in the way $c(2c^2\mathbf{1} + E\mathbf{1} - \mathcal{V})^{-1}$ is expanded. To account for these varying schemes, we expand the relativistic corrections as

$$\frac{1E - \mathcal{V}}{2c^2} = \frac{\mathcal{R}}{2c^2} = \frac{1 + \mathcal{R}^{(0)}}{2c^2} \tilde{\mathcal{R}}^{-1} - \mathbf{1}. \quad (16)$$

Here $\mathcal{R}^{(0)}$ is both α and energy independent, whereas $\tilde{\mathcal{R}}$ contains all α and energy dependence. Therefore we can write

$$\psi_{2c}^{\text{S}} \approx c(2c^2\mathbf{1} + \mathcal{R}^{(0)})^{-1} \tilde{\mathcal{R}} \tilde{\sigma} \cdot \hat{p} \psi_{2c}^{\text{L}}. \quad (17)$$

This separation allows for a simultaneous treatment of e. g. the Pauli expansion and a regular approximation

ansatz, where for zeroth order Hamiltonians $\tilde{\mathcal{R}}$ reduces to $\mathbf{1}$. The quasi-relativistic Hamiltonian operators may then be written in the general form

$$\hat{H}_{2c} = c^2 \tilde{\sigma} \cdot \hat{p} \left(2c^2\mathbf{1} + \mathcal{R}^{(0)} \right)^{-1} \tilde{\mathcal{R}} \tilde{\sigma} \cdot \hat{p} + \hat{V}. \quad (18)$$

Note that methods relying on a resolution-of-the-identity expansion, like the so-called exactly transformed two-component Hamiltonians (X2C), can principally also start from this formulation. The direct connection may become more apparent, if a symmetric elimination of the small component is considered leading to the Hamiltonian

$$\begin{aligned} \hat{H}_{2c,\text{sym}} &= \hat{V} + c^2 \tilde{\sigma} \cdot \hat{p} \left[(\tilde{\mathcal{R}})^\dagger \left(2c^2\mathbf{1} + \mathcal{R}^{(0)} \right)^{-1} \right. \\ &\quad \left. + \left(2c^2\mathbf{1} + \mathcal{R}^{(0)} \right)^{-1} \tilde{\mathcal{R}} \right] \tilde{\sigma} \cdot \hat{p} \\ &\quad + \tilde{\sigma} \cdot \hat{p} (\tilde{\mathcal{R}})^\dagger \left(2c^2\mathbf{1} + \mathcal{R}^{(0)} \right)^{-1} \\ &\quad \times \hat{V} \left(2c^2\mathbf{1} + \mathcal{R}^{(0)} \right)^{-1} \tilde{\mathcal{R}} \tilde{\sigma} \cdot \hat{p}. \end{aligned} \quad (19)$$

Under a variation of the fine-structure constant the 2c Hamiltonians become

$$\hat{H}_{2c} = \tilde{\sigma} \cdot \hat{p} \left(2 \times \mathbf{1} + (\alpha + \delta\alpha)^2 \mathcal{R}^{(0)} \right)^{-1} \tilde{\mathcal{R}} \tilde{\sigma} \cdot \hat{p} + \hat{V}. \quad (20)$$

and

$$\begin{aligned} \hat{H}_{2c,\text{sym}} &= \hat{V} + \tilde{\sigma} \cdot \hat{p} \left[(\tilde{\mathcal{R}})^\dagger \left(2 \times \mathbf{1} + (\alpha + \delta\alpha)^2 \mathcal{R}^{(0)} \right)^{-1} \right. \\ &\quad \left. + \left(2 \times \mathbf{1} + (\alpha + \delta\alpha)^2 \mathcal{R}^{(0)} \right)^{-1} \tilde{\mathcal{R}} \right] \tilde{\sigma} \cdot \hat{p} \\ &\quad + (\alpha + \delta\alpha)^4 \tilde{\sigma} \cdot \hat{p} (\tilde{\mathcal{R}})^\dagger \left(2 \times \mathbf{1} + (\alpha + \delta\alpha)^2 \mathcal{R}^{(0)} \right)^{-1} \\ &\quad \times \hat{V} \left(2 \times \mathbf{1} + (\alpha + \delta\alpha)^2 \mathcal{R}^{(0)} \right)^{-1} \tilde{\mathcal{R}} \tilde{\sigma} \cdot \hat{p}. \end{aligned} \quad (21)$$

Here it must be remembered that $\tilde{\mathcal{R}}_{2c}$ also depends on the variation of α . Now we repeat the steps we did for the DC-Hamiltonian. Assuming that $2c^2\mathbf{1} + \mathcal{R}^{(0)}$ is invertible and that the series

$$\tilde{\mathcal{R}}(\tilde{x}) = \sum_{k=0}^{\infty} \underbrace{\left. \frac{\partial^k \tilde{\mathcal{R}}}{\partial \tilde{x}^k} \right|_{\delta\alpha=0}}_{\tilde{\mathcal{R}}^{(k)}} \tilde{x}^k \quad (22)$$

converges, we can expand the inverse of the expression in parenthesis in eq. (20) and the transformation matrix $\tilde{\mathcal{R}}$ in \tilde{x} :

$$\begin{aligned}
\hat{H}_{2c} &= \underbrace{\vec{\sigma} \cdot \hat{p} c^2 \omega \tilde{\mathcal{R}} \vec{\sigma} \cdot \hat{p}}_{\hat{H}_{2c}} + \hat{V} \\
&+ \underbrace{\vec{\sigma} \cdot \hat{p} c^2 \omega \sum_{k=1}^{\infty} \left[\tilde{x}^k \left[\left(-\mathcal{R}^{(0)} \omega \right)^k \left((1 - \delta_{k-1,0}) \tilde{\mathcal{R}}^{(0)} + \tilde{\mathcal{R}}^{(k-1)} \right) + \tilde{\mathcal{R}}^{(k)} \left(1 - \delta_{k-1,0} + \left(-\mathcal{R}^{(0)} \omega \right)^{k-1} \right) \right] \right]}_{\hat{H}_{2c}(\delta\alpha)} \vec{\sigma} \cdot \hat{p},
\end{aligned} \tag{23}$$

where we introduced the zeroth order transformation matrix operator $c^2 \omega = \left(2 \times \mathbf{1} + \alpha^2 \mathcal{R}^{(0)} \right)^{-1}$

In case of one-particle regular expansions $\mathcal{R}^{(0)}$ reduces to $-\hat{V} \times \mathbf{1}$ and $\tilde{\mathcal{R}}$ is of the form $\sum_{k=0}^n \left[\frac{-E}{2c^2 - \tilde{V}} \right]^k \times \mathbf{1}$ for order n of the regular approximation. We will focus on zeroth order (ZORA) using van Wüllen's model potential \tilde{V} [25], such that $\mathcal{R}^{(0)}$ reduces to the scalar potential $-\tilde{V}$ and the inverse matrix ω reduces to the scalar $\omega = \left(2c^2 - \tilde{V} \right)^{-1}$. We obtain for the first and second order perturbations in \tilde{x}

$$\hat{H}_{\text{ZORA}}^{(1)} = \vec{\sigma} \cdot \hat{p} c^2 \omega^2 \tilde{V} \vec{\sigma} \cdot \hat{p} \tag{24}$$

$$\hat{H}_{\text{ZORA}}^{(2)} = 2 \vec{\sigma} \cdot \hat{p} c^2 \omega^3 \tilde{V}^2 \vec{\sigma} \cdot \hat{p}. \tag{25}$$

To show consistency with the four-component expressions, we start from the first and second order perturbing operators in the Dirac picture [eqs. (12) and (15)] and insert the ZORA approximation $\psi^S \rightarrow c \omega \vec{\sigma} \cdot \hat{p} \psi_{\text{ZORA}}$:

$$\hat{H}_{\text{D,ZORA}}^{(1)} = -\vec{\sigma} \cdot \hat{p} c^2 \omega \vec{\sigma} \cdot \hat{p} + 2c^4 \vec{\sigma} \cdot \hat{p} \omega^2 \vec{\sigma} \cdot \hat{p} \tag{26}$$

$$\begin{aligned}
\hat{H}_{\text{D,ZORA}}^{(2)} &= \frac{3}{2} \vec{\sigma} \cdot \hat{p} c^2 \omega \vec{\sigma} \cdot \hat{p} - 4c^4 \vec{\sigma} \cdot \hat{p} \omega^2 \vec{\sigma} \cdot \hat{p} \\
&+ \frac{1}{2} \vec{\sigma} \cdot \hat{p} c^2 \omega \vec{\sigma} \cdot \hat{p} - 4c^4 \vec{\sigma} \cdot \hat{p} \omega^2 \vec{\sigma} \cdot \hat{p} \\
&+ 8c^6 \vec{\sigma} \cdot \hat{p} \omega^3 \vec{\sigma} \cdot \hat{p},
\end{aligned} \tag{27}$$

where the last three terms of $\hat{H}_{\text{D,ZORA}}^{(2)}$ are diamagnetic-like contributions that stem from products of $\hat{H}_{\text{D,ZORA}}^{(1)}$ that are of second order in \tilde{x} in the transformation from the DC-Hamiltonian to ZORA. This is in agreement with eq. (24), as by using $\omega = \frac{1}{2c^2} (1 + \tilde{V} \omega)$ we receive

$$\begin{aligned}
\hat{H}_{\text{D,ZORA}}^{(1)} &= c^2 \vec{\sigma} \cdot \hat{p} \omega (2c^2 \omega - 1) \vec{\sigma} \cdot \hat{p} \\
&= \vec{\sigma} \cdot \hat{p} c^2 \omega^2 \tilde{V} \vec{\sigma} \cdot \hat{p}
\end{aligned} \tag{28}$$

$$\begin{aligned}
\hat{H}_{\text{D,ZORA}}^{(2)} &= 2c^2 \vec{\sigma} \cdot \hat{p} \omega (1 - 4c^2 \omega + 4c^4 \omega^2) \vec{\sigma} \cdot \hat{p} \\
&= 2c^2 \vec{\sigma} \cdot \hat{p} \omega (1 - 2c^2 \omega)^2 \vec{\sigma} \cdot \hat{p} \\
&= 2 \vec{\sigma} \cdot \hat{p} c^2 \omega^3 \tilde{V}^2 \vec{\sigma} \cdot \hat{p}.
\end{aligned} \tag{29}$$

Finally, it can be easily seen that the chosen expansion in \tilde{x} is equivalent to the Pauli-like expansion of the Dirac equation. For higher orders in \tilde{x} the present scheme could be related to the linear response with elimination of small

components (LRESC) [26], which is designed to capture all corrections of a given order in \tilde{x} including those not included in the DC picture such as the Breit interaction or virtual pair creation. Using eq. (23) we can relate different orders of the Pauli Hamiltonian to different orders in \tilde{x} : Within the Pauli-like expansion \mathcal{R} vanishes and in k th order we have

$$\tilde{\mathcal{R}}_{\text{Pauli}}^{(k)} = \left(\frac{V - E}{2c^2} \right)^k \tag{30}$$

yielding the perturbing operators

$$\hat{H}_{\text{Pauli}}^{(1)} = \vec{\sigma} \cdot \hat{p} \frac{V - E}{4c^2} \vec{\sigma} \cdot \hat{p} \tag{31}$$

$$\hat{H}_{\text{Pauli}}^{(2)} = \vec{\sigma} \cdot \hat{p} \frac{(V - E)^2}{4c^4} \vec{\sigma} \cdot \hat{p}, \tag{32}$$

which are, as expected, just the relativistic corrections of different order in the Pauli expansion.

III. COMPUTATIONAL DETAILS

Quasi-relativistic two-component calculations within the zeroth order regular approximation (ZORA) were performed with a modified version [20, 27–32] of a two-component program [33] based on Turbomole [34] on the level of complex generalized Hartree–Fock (cGHF). The gauge dependence of the ZORA Hamiltonian was alleviated by a model potential as suggested by van Wüllen [25] which was applied with additional damping [35].

Orbitals for excited Slater determinants were obtained by choosing the occupation numbers in the SCF calculations to achieve maximum overlap with the determinant of the previous cycle (maximum overlap method, MOM) as described e.g. in Ref. [36]. In case that a change in the differential density compared to the previous cycle was above $10^{-3}/a_0^{-3}$ the occupation numbers were chosen such that the maximum overlap of the determinant with respect to the initial guess is achieved (initial guess MOM, IMOM) [36, 37]. The initial guess was generated by reoccupation of the cGHF orbitals (occupied and virtual) obtained for the cGHF determinant of lowest energy.

Expectation values of operators (24) and (25) were computed via the toolbox approach outlined in Ref. [30]. Within the quasi-relativistic ZORA framework, the second order expression in eq. (14) was computed at the

level of coupled perturbed HF as outlined in Refs. [30–32].

Transition electric dipole moments $\bar{\mu}^{f\leftarrow i}$ were computed using the independently obtained cGHF determinants of the different states using Löwdin rules [38] for single-particle operator transition matrix elements between non-orthogonal single-determinantal initial (i) wave function Φ_i and final (f) wave function Φ_f (see also Ref. [39]):

$$\bar{\mu}^{f\leftarrow i} = \left\langle \Phi_f \left| \sum_k q_k \vec{r}_k \right| \Phi_i \right\rangle \quad (33)$$

$$= \sum_{ij} \langle \psi_{f,i} | -|e|\vec{r}| \psi_{i,j} \rangle \text{adj}(\mathbf{S})_{ij} + \sum_A Z_A |e|\vec{r}_A \det \mathbf{S}. \quad (34)$$

Here, the index k runs over all electrons and nuclei with charges q_k , whereas A runs over all nuclei with nuclear charge number Z_A . \mathbf{S} is the overlap matrix between the molecular spinors ψ_i and ψ_j forming the initial and the final state Slater determinant, respectively, with corresponding matrix elements $S_{ij} = \langle \psi_{f,i} | \psi_{i,j} \rangle$. The symbol $\det \mathbf{S}$ denotes the determinant of the matrix \mathbf{S} , whereas $\text{adj}(\mathbf{S})$ denotes the adjugate of \mathbf{S} . Wavefunctions were optimized until a change in energy lower than $10^{-9} E_h$ and in relative spin-orbit coupling energy contribution lower than 10^{-11} was achieved. Optimizations of bond lengths were performed until a change in energy of $10^{-6} E_h$ or lower was reached. Coupled perturbed HF equations were solved iteratively until we obtained a norm of the residuum of 10^{-6} or lower (see Ref. [31] for details of the implementation).

Relativistic four component calculations employing the DC-Hamiltonian were performed with the quantum chemistry program package Dirac [19]. The various states computed on the level of average-of-configuration (AOC) Dirac–Hartree–Fock (DHF) were obtained in a MOM kind of approach while treating the open-shell systems within the AOC framework. Four component relativistic Fock-space coupled-cluster calculations with singles and doubles cluster amplitudes (FSCCSD) were performed with the ground state wavefunction of the closed shell CeF^{3+} system as reference and attaching one additional electron (0-1 sector). For FSCCSD calculations an active space with seven electrons of F ($2s^2 2p^5$) and 19 electrons of Ce ($4d^{10} 5s^2 5p^6 4f^1$) and virtual spinors up to an energy of $50 E_h$ was employed. PaF^{3+} was treated as described in [20]. AOC-DHF spinors were optimized until a change in the orbital gradient 10^{-8} or lower was reached.

In all calculations with CeF^{2+} Dyall’s core-valence triple- ζ (Dyall-cv3z) basis set was employed for Ce and F [40–42]. In Ref. [43] we employed a similar basis set in the two-component ZORA-cGHF computations of CeF^{2+} , but therein with additional steep s and p functions. Those additional steep functions weakly impact on the electronic properties computed in our present work. Consequently, also potential energy curves with

similar shapes and similar spectroscopic constants derived from these potential energy curves (see Tab. II) result. For completeness, we provide the present raw data of the potential energy curves (computed at $c = c_0 = 137.0359895 a_0 E_h \hbar^{-1}$) in the Supplemental Material [44] and display therein also the corresponding potential energy curves.

For the computation of PaF^{3+} we followed Ref. [20] and used in two-component calculations with PaF^{3+} a basis set consisting of 37s, 34p, 14d and 9f uncontracted Gaussian functions for Pa. The basis set is constructed as an even-tempered series as $\alpha_i = a/b^{i-1}$; $i = 1, \dots, N$, with the exponential coefficients α_i and N as the number of functions, with $b = 2$ for s and p functions and $b = (5/2)^{1/25} \times 10^{2/5} \approx 2.6$ for d and f functions. The corresponding largest exponent coefficients a of the subsets are $2 \times 10^9 a_0^{-2}$ (s), $5 \times 10^8 a_0^{-2}$ (p), $13300.758 a_0^{-2}$ (d) and $751.8368350 a_0^{-2}$ (f). For the F atom in these ZORA-cGHF computations a decontracted atomic natural orbital basis set of double- ζ quality augmented with polarization valence basis functions (ANO-RCC-VDZP) [45] was employed. We note that, in contrast to Ref. [20], a wavefunction fulfilling tighter convergence criteria in the spin-orbit coupling contribution was required for the subsequent response calculations.

In all two- and four-component calculations a normalized spherical Gaussian nuclear density distribution $\rho_A(\vec{r}) = \frac{\zeta_A^{3/2}}{\pi^{3/2}} e^{-\zeta_A |\vec{r} - \vec{r}_A|^2}$ with corresponding charge distribution $Z_A e \rho_A(\vec{r})$ was employed with $\zeta_A = \frac{3}{2r_{\text{nuc},A}^2}$, and the root-mean-square radius $r_{\text{nuc},A}$ chosen as suggested by Visscher and Dyall [46] with the isotopes ^{140}Ce , ^{231}Pa and ^{19}F .

To obtain for comparison to our perturbative approach the sensitivity to variations of α also numerically, we altered the speed of light c , which is (in atomic units) $c/(a_0 E_h \hbar^{-1}) = 1/\alpha = 137.0359895$, to take the values $125.0359895 + n$ where n are integer values from 0 to 26. To densify the region around $c/(a_0 E_h \hbar^{-1}) = 137.0359895$ we further included the values 136.6359895, 136.7359895, 136.8359895, 136.9359895, 137.1359895, 137.2359895, 137.3359895, 137.4359895 on the level of ZORA-cGHF and AOC-DHF. For the FSCCSD calculations we varied $c/(a_0 E_h \hbar^{-1})$ to take the values 125.0359895, 127.0359895, 129.0359895, 131.0359895, 133.0359895, 135.0359895, 137.0359895, 140.0359895, 143.0359895, 146.0359895, 149.0359895, 152.0359895. The sensitivity parameters are then obtained via a fit to a 4th order polynomial. As fitting procedure a non-linear least squares Marquardt–Levenberg algorithm as implemented in GNUPLLOT [47] was employed. We report numerical data and raw data from the outputs of the calculations in the Supplemental Material [44].

From the potential energy curves electronic excitation wavenumbers $\tilde{\nu}$, equilibrium bond lengths r_e and harmonic vibrational wavenumbers $\tilde{\omega}_e$ are obtained by fitting a harmonic oscillator potential around the potential minimum (data points are listed in Supplemental Mate-

Table I. Grid point parameters for the DVR for the different electronic states. The evenly spaced grid starts from the internuclear distance r_{lowest} and is increased in increments of r_{step} to reach the total number of grid points n .

| State | CeF ²⁺ | | | PaF ³⁺ | | |
|--------|--------------------------------|------------------------------|------|--------------------------------|-----------------------------|------|
| | $r_{\text{lowest}}/\text{\AA}$ | $r_{\text{step}}/\text{\AA}$ | n | $r_{\text{lowest}}/\text{\AA}$ | $r_{\text{step}}/\text{pm}$ | n |
| (X)5/2 | 1.34 | 0.001 | 2400 | 1.3 | 0.175 | 1000 |
| (1)3/2 | 1.34 | 0.001 | 2400 | 0.95 | 0.100 | 1900 |
| (1)1/2 | 1.34 | 0.001 | 2400 | 0.95 | 0.100 | 2000 |
| (1)7/2 | 1.34 | 0.001 | 2400 | 0.95 | 0.100 | 2090 |
| (1)5/2 | 1.34 | 0.001 | 2400 | 0.95 | 0.100 | 2090 |
| (2)3/2 | 1.34 | 0.001 | 2400 | 0.95 | 0.100 | 2090 |
| (2)1/2 | 1.34 | 0.001 | 2400 | 1.15 | 0.100 | 1850 |
| (3)3/2 | 1.34 | 0.001 | 1910 | 1.40 | 0.100 | 950 |

rial [44]).

For a vibronic transition analysis vibrational corrections to the property q_1 are computed by solving the vibrational Schrödinger equation in a one-dimensional discrete variable representation (DVR) approach on an equidistant grid [48]. The corresponding grid points for each state are given in Tab. I. We interpolate q_1 as a polynomial function of the bond length of order three for the electronic ground state and of order five for electronic excited states as described e.g. in the Supplemental Material of Ref. [49]. Natural linewidths Γ_{iv} are approximated by taking the sum of the Einstein coefficients A_{ju} of all decay channels from the considered excited state (in SI units)

$$\Gamma_{iv} = \sum_{ju} \theta(E_{iv} - E_{ju}) A_{ju,iv} \quad (35)$$

$$= \sum_{ju} \theta(E_{iv} - E_{ju}) \frac{8\pi^2 \tilde{\nu}_{ju,iv}^3}{3\epsilon_0 c^3 \hbar} |\bar{\mu}_{ju,iv}^2| \quad (36)$$

with the electric constant ϵ_0 and the reduced Planck constant \hbar . The transitions are defined through the vibrational (u, v) and electronic (j, i) state. Here, we used a left-continuous Heaviside-function $\theta(E_{iv} - E_{ju})$ that yields 0, when the energetic difference $E_{iv} - E_{ju}$ between the vibronic levels is zero or lower, and 1 otherwise. The vibronic electric transition dipole moment $\bar{\mu}_{ju,iv}$ is estimated by multiplying the Franck-Condon factor of the transition $f^{(ju,iv)}$ with the squared electronic transition dipole moment $\bar{\mu}^{j \leftarrow i}$ computed at the equilibrium structure.

IV. RESULTS

A. Electronic states of CeF²⁺ and PaF³⁺

The electronic structure of PaF³⁺ was discussed in detail in Ref. [20]. For completeness we present herein again spectroscopic properties of the eight energetically lowest electronic states in PaF³⁺ and compare them to

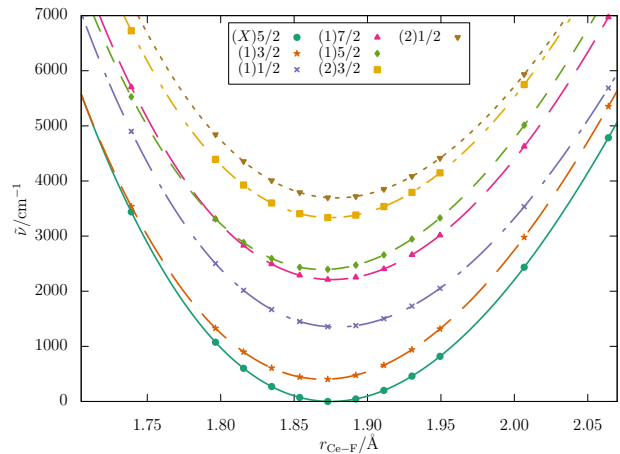


Figure 1. Potential energy curves for the seven energetically lowest electronic states relative to the energetic minimum of the electronic ground state of CeF²⁺ computed on the level of DC-FSCCSD.

the electronic states of CeF²⁺ in Table II. For CeF²⁺ we emphasise, that the basis set employed herein in the two-component ZORA-cGHF calculations is similar to the basis set employed in Ref. [43], but omits the additional steep s and p functions. This similarity of basis sets for CeF²⁺ results in nearly identical potential energy shapes obtained on the level of ZORA-cGHF compared to Ref. [43] (see computational details). In the present paper we additionally report potential energy curves computed on the level of FSCCSD of CeF²⁺ (Fig. 1). Derived from the potential energy curves, we obtain relevant spectroscopic properties that are compared in Tab. II.

As previously analysed in Ref. [43], CeF²⁺ has a similar electronic structure as PaF³⁺ and only slightly shorter bond lengths. Furthermore, in CeF²⁺ the energetically lowest seven electronic states are even closer to each other in energy than in PaF³⁺. The agreement between ZORA-cGHF and FSCCSD is similar as in PaF³⁺: ZORA-cGHF gives in general reasonable results, with all vertical excitation wavenumbers appearing slightly overestimated by the mean field approach. This effect is larger for the lower states computed with AOC-DHF due to lacking spin-polarisation in the AOC-DHF approach.

B. Analytical vs. numerical computation of α -variations in CeF²⁺

We demonstrate the applicability of the analytic derivatives with respect to $\delta\alpha$ by comparison to numerical variations of the fine structure constant in AOC-DHF and ZORA-cGHF calculations. The comparison between the numerical and analytical results is presented in Tab. III (the corresponding vertical excitation energies as a function of α are shown in Figures 2 to 4).

All numerical results for Δq_1 are in excellent agreement with the analytical calculations. The comparison

Table II. Equilibrium bond lengths r_e , vertical excitation wavenumber $\tilde{\nu}$ from the electronic ground state minimum and harmonic vibrational wavenumber $\tilde{\omega}_e$ of CeF^{2+} as obtained from potential energy curves on the level of ZORA-cGHF, AOC-DHF and FSCCSD. We received for CeF^{2+} on the ZORA-cGHF level values that are within the reported number of digits identical to those computed in Ref. [43] with a basis set that was augmented by additional steep s and p functions (see computational details for different basis sets employed). Where available data are compared to PaF^{3+} from Ref. [20]. We note that the basis sets employed for CeF^{2+} and PaF^{3+} differ in their quality.

| State | Method | CeF^{2+} | | | PaF^{3+} [20] | | |
|--------|-----------|-------------------|------------------------------|-----------------------------------|------------------------|------------------------------|-----------------------------------|
| | | $r_e/\text{\AA}$ | $\tilde{\nu}/\text{cm}^{-1}$ | $\tilde{\omega}_e/\text{cm}^{-1}$ | $r_e/\text{\AA}$ | $\tilde{\nu}/\text{cm}^{-1}$ | $\tilde{\omega}_e/\text{cm}^{-1}$ |
| (X)5/2 | ZORA-cGHF | 1.91 | — | 722 | 1.87 | — | 846 ⁽¹⁾ |
| | AOC-DHF | 1.91 | — | 722 | | | |
| | FSCCSD | 1.88 | — | 803 | 1.85 | — | 859 |
| (1)3/2 | ZORA-cGHF | 1.91 | 1050 | 718 | 1.86 | 1250 | 842 ⁽¹⁾ |
| | AOC-DHF | 1.91 | 1220 | 716 | | | |
| | FSCCSD | 1.88 | 404 | 803 | 1.84 | 658 | 844 |
| (1)1/2 | ZORA-cGHF | 1.91 | 1460 | 716 | 1.87 | 3020 | 838 ⁽¹⁾ |
| | AOC-DHF | 1.91 | 1860 | 716 | | | |
| | FSCCSD | 1.88 | 1360 | 788 | 1.86 | 3060 | 861 |
| (1)7/2 | ZORA-cGHF | 1.91 | 2300 | 723 | 1.87 | 5520 | 846 ⁽¹⁾ |
| | AOC-DHF | 1.91 | 2130 | 722 | | | |
| | FSCCSD | 1.88 | 2210 | 804 | 1.85 | 5540 | 861 |
| (1)5/2 | ZORA-cGHF | 1.91 | 3310 | 720 | 1.86 | 6440 | 845 ⁽¹⁾ |
| | AOC-DHF | 1.91 | 3240 | 715 | | | |
| | FSCCSD | 1.87 | 2400 | 801 | 1.84 | 5790 | 846 |
| (2)3/2 | ZORA-cGHF | 1.91 | 3770 | 718 | 1.87 | 8000 | 841 ⁽¹⁾ |
| | AOC-DHF | 1.91 | 3820 | 717 | | | |
| | FSCCSD | 1.88 | 3340 | 798 | 1.85 | 7810 | 853 |
| (2)1/2 | ZORA-cGHF | 1.91 | 3930 | 716 | 1.87 | 8820 | 840 ⁽¹⁾ |
| | AOC-DHF | 1.92 | 4230 | 718 | | | |
| | FSCCSD | 1.88 | 3700 | 791 | 1.86 | 8940 | 858 |
| (3)3/2 | ZORA-cGHF | 1.85 | 31 900 | 774 | 1.83 | 30 000 | 888 ⁽¹⁾ |
| | AOC-DHF | 1.85 | 31 300 | 755 | | | |
| | FSCCSD | 1.88 | 27 900 | 791 | 1.83 | 29 200 | 882 |

⁽¹⁾ The harmonic vibrational wavenumbers for PaF^{3+} on the level of ZORA-cGHF are obtained herein by fitting a third order polynomial to the numerically calculated potential energy curve from Ref. [20], whereas in Ref. [20] a second order polynomial was used. This causes small numerical differences in the reported values. Both fit procedures only use data points around the respective equilibrium bond lengths.

between analytic and numeric approach of the second order parameter Δq_2 is only done at the level of ZORA-cGHF as in the program package DIRAC open-shell linear response calculations are not available. The values of Δq_1 computed on the level of ZORA-cGHF deviate from values computed on the level of AOC-DHF by $\lesssim 13\%$. This deviation is partially explainable by the different HF approaches used in ZORA-cGHF and AOC-DHF calculations, which is also reflected in the deviation of the excitation wavenumbers in Tab. II. Deviations are even

larger for q_2 , which may depend more strongly on the choice of the relativistic Hamiltonian, as it may include two-electron exchange contributions from spin-orbit coupling which we neglect in our ZORA calculations. Moreover, the different HF method, i.e. AOC-HF and cGHF, include correlation effects to some extent but in very different ways. To gauge errors of both HF approaches we performed more sophisticated FSCCSD calculations of q_1 and q_2 using the numerical approach (Tab. IV).

FSCCSD results for Δq_1 are in reasonable agreement

Table III. Analytically (an.) and numerically (num.) determined results for the sensitivity parameters Δq_1 and Δq_2 for CeF^{2+} computed on the level of ZORA-cGHF and AOC-DHF. The relative deviation between ZORA-cGHF and AOC-DHF was computed as $\text{dev.}_{4c,2c} = 1 - \frac{\Delta q_{\text{ZORA-cGHF}}}{\Delta q_{\text{AOC-DHF}}}$, where in case of Δq_1 the analytical values were used and in case of Δq_2 the analytical value from ZORA-cGHF and the numerical value from AOC-DHF. For the (3)3/2 electronic state only analytical results are computed. For each method and each electronic state the corresponding equilibrium bond length was used as internuclear distance (see Supplemental Material).

| State | Method | $\Delta q_1/\text{cm}^{-1}$ | | | $\Delta q_2/\text{cm}^{-1}$ | | |
|--------|-----------|-----------------------------|--------|--------------------------|-----------------------------|------|--------------------------|
| | | an. | num. | dev. _{4c,2c} /% | an. | num. | dev. _{4c,2c} /% |
| (1)3/2 | ZORA-cGHF | 123.3 | 123.3 | 7.3 | -32 | -31 | 48.4 |
| | AOC-DHF | 133.0 | 133.0 | | — | -61 | |
| (1)1/2 | ZORA-cGHF | -222.9 | -222.9 | -10.8 | -272 | -272 | 35.6 |
| | AOC-DHF | -201.3 | -201.3 | | — | -423 | |
| (1)7/2 | ZORA-cGHF | 2023.2 | 2023.3 | -8.5 | -727 | -727 | -8.6 |
| | AOC-DHF | 1865.6 | 1865.6 | | — | -669 | |
| (1)5/2 | ZORA-cGHF | 2186.2 | 2186.3 | -8.0 | -734 | -734 | -8.0 |
| | AOC-DHF | 2024.1 | 2024.1 | | — | -679 | |
| (2)3/2 | ZORA-cGHF | 2078.3 | 2078.3 | -7.9 | -867 | -867 | -5.1 |
| | AOC-DHF | 1926.6 | 1926.6 | | — | -825 | |
| (2)1/2 | ZORA-cGHF | 1744.7 | 1744.8 | -12.7 | -998 | -998 | -4.8 |
| | AOC-DHF | 1547.8 | 1547.8 | | — | -953 | |
| (3)3/2 | ZORA-cGHF | -23 863 | — | 1.7 | -2434 | — | — |
| | AOC-DHF | -24 283 | — | | — | — | |

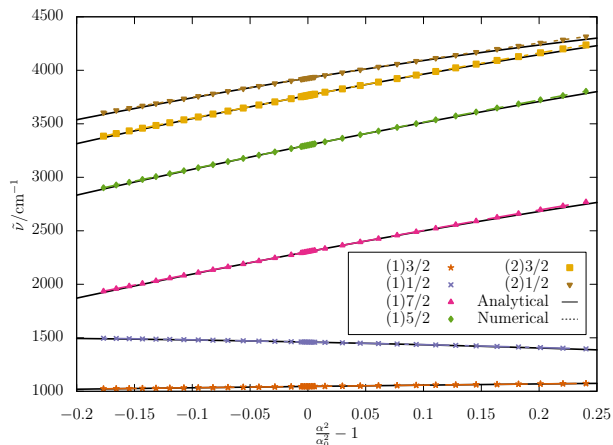


Figure 2. Adiabatic excitation energy of CeF^{2+} as a function of the variation in α computed on the ZORA-cGHF level. The bond lengths for the different electronic states are listed in Tab. II and were not changed when varying α . Dots correspond to the values obtained when changing α numerically with the corresponding 4th order polynomial fit shown as dashed lines. Solid lines correspond to the analytically obtained second order expansion with Δq_1 and Δq_2 values from Tab. III.

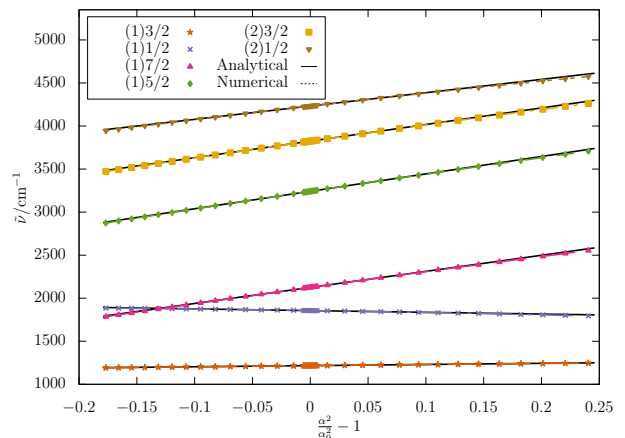


Figure 3. Adiabatic excitation energy of CeF^{2+} as a function of the variation in α computed on the AOC-DHF level. The bond lengths for the different electronic states are listed in Tab. II and were not changed when varying α . Dots correspond to the values obtained when changing α numerically with the corresponding 4th order polynomial fit shown as dashed lines. Solid lines correspond to the analytically obtained second order expansion with Δq_1 and Δq_2 values from Tab. III.

with ZORA-cGHF. Deviations for Δq_2 are larger, which may in part be attributed to the stronger dependence on two-electron exchange contributions to spin-orbit cou-

pling.

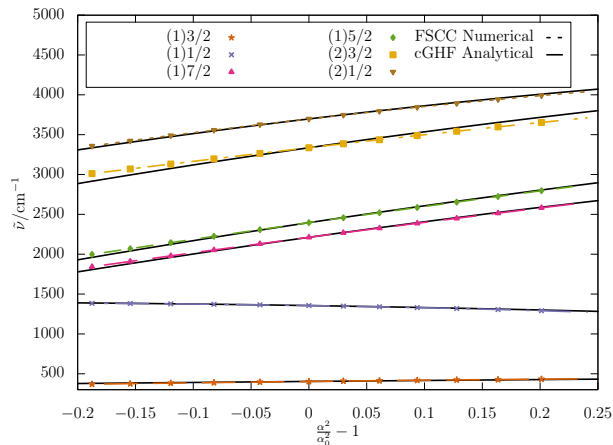


Figure 4. Adiabatic excitation energy of CeF^{2+} as a function of the variation in α computed on the FSCSD level. The bond lengths for the different electronic states are listed in Tab. II and were not changed when varying α . Dots correspond to the values obtained when changing α numerically with the corresponding 4th order polynomial fit shown as dashed lines. For comparison, curves with slopes and curvatures obtained analytically obtained on the ZORA-cGHF level are shown with their y-intercepts set to the corresponding FSCSD values.

Table IV. Numerical results for the sensitivity parameters Δq_1 and Δq_2 for CeF^{2+} computed on the level of FSCSD compared to the results computed on the level of AOC-DHF and ZORA-cGHF with the electronic ground state as reference. The relative deviations were computed as $\text{dev.}_{\text{method}} = 1 - \frac{\Delta q_{\text{method}}}{\Delta q_{\text{FSCSD}}}$. For ZORA-cGHF and AOC-DHF the equilibrium bond lengths for each respective electronic state was used, while in FSCSD the internuclear distance was set for all electronic states to the AOC-DHF equilibrium value of the electronic ground state (see Supplemental Material [44]).

| State | $\Delta q_{1,\text{FSCSD}}$ | $\Delta q_{2,\text{FSCSD}}$ | $\Delta q_{1,\text{DHF}}^{\text{dev.}}/\%$ | $\Delta q_{1,\text{cGHF}}^{\text{dev.}}/\%$ | $\Delta q_{2,\text{cGHF}}^{\text{dev.}}/\%$ |
|--------|-----------------------------|-----------------------------|--|---|---|
| (1)3/2 | 163.9 | -191 | 18.9 | 24.8 | 83.4 |
| (1)1/2 | -229.5 | -859 | 12.3 | 2.9 | 68.3 |
| (1)7/2 | 1907.8 | -668 | 2.2 | -6.1 | -8.8 |
| (1)5/2 | 2061.5 | -665 | 1.8 | -6.0 | -10.4 |
| (2)3/2 | 1671.2 | -781 | -15.3 | -24.4 | -11.0 |
| (2)1/2 | 1639.6 | -1821 | 5.6 | -6.4 | 45.2 |
| (3)3/2 | -19114 | -4449 | -27.0 | -24.8 | -54.9 |

C. Enhancement of variations of fundamental constants in vibronic transitions of CeF^{2+} and PaF^{3+}

Both molecular ions CeF^{2+} and PaF^{3+} possess several energetically close lying electronic states. Consequently, a huge variety of accidentally nearly degenerate vibronic transitions can be expected. Particular interesting is the region in which the vibrational levels of the energetically lowest seven potentials, which are dominated by an unpaired f-like electron located at Ce or Pa, are close to the vibrational levels of the seventh excited states, which is dominated by an unpaired d-like electron located at Ce or Pa (see discussion in Ref. [20] and Fig. 5). In an experiment, nearly degenerate levels can be used [50] to compare transitions from a reference state into these

Table V. Analytically determined results for the sensitivity parameters Δq_1 and Δq_2 for PaF^{3+} computed on the level of ZORA-cGHF. For each electronic state the corresponding equilibrium bond length was used as internuclear distance (see Supplemental Material).

| State | $\Delta q_1/\text{cm}^{-1}$ | $\Delta q_2/\text{cm}^{-1}$ |
|--------|-----------------------------|-----------------------------|
| (1)3/2 | 738.3 | -1426 |
| (1)1/2 | -2101.6 | -5366 |
| (1)7/2 | 3473.6 | -4910 |
| (1)5/2 | 4341.2 | -5645 |
| (2)3/2 | 2806.5 | -9261 |
| (2)1/2 | 690.1 | -9579 |
| (3)3/2 | -42839.0 | -1571 |

states and to measure the difference of both transition wavenumbers

$$\Delta \tilde{\nu}_{iv,jw} = \tilde{\nu}_{iv} - \tilde{\nu}_{jw} \quad (37)$$

and its variation over time

$$\begin{aligned} \frac{\delta \Delta \tilde{\nu}_{iv,jw}}{\Delta \tilde{\nu}_{iv,jw}} &= (K_{\alpha,iv} - K_{\alpha,jw}) \frac{\delta \alpha}{\alpha} + (K_{\mu,iv} - K_{\mu,jw}) \frac{\delta \mu}{\mu} \\ &= \Delta K_{\alpha,iv,jw} \frac{\delta \alpha}{\alpha} + \Delta K_{\mu,iv,jw} \frac{\delta \mu}{\mu} \end{aligned} \quad (38)$$

The importance of the close lying states for large enhancements of a hypothetical α variation is e. g. demonstrated with the literature known atomic clock Yb [51–53]. The Δq_1 values for transitions from the Yb ground state to excited electronic states are in the range of 1000 cm^{-1} and -40000 cm^{-1} [5]. We predicted here similar values for PaF^{3+} . Due to the large differences in energy of the levels in Yb, the absolute values of the enhancement factors K are reduced to below 15. In molecular systems, however, orders of magnitude higher absolute values of K are in principle found regularly as a result of the quasi degenerate vibrational states.

Measuring corresponding wavenumber differences very accurately is in principle possible under favourable circumstances with the help of frequency combs (see e.g. Refs. [54] and [6]).

This requires, however, that the absorption linewidths are rather narrow in order to resolve close lying transitions. For our current estimates of the linewidths we restricted ourselves to the electric dipole approximation (see computational details). For a more accurate estimate, however, higher order terms (magnetic dipole, electric quadrupole, etc.) would have to be included.

1. CeF^{2+}

From the vibrationally corrected $\Delta q_{1,i}$ values ($\Delta q_{1,iv}$) and the electronic and vibrational transition wavenum-

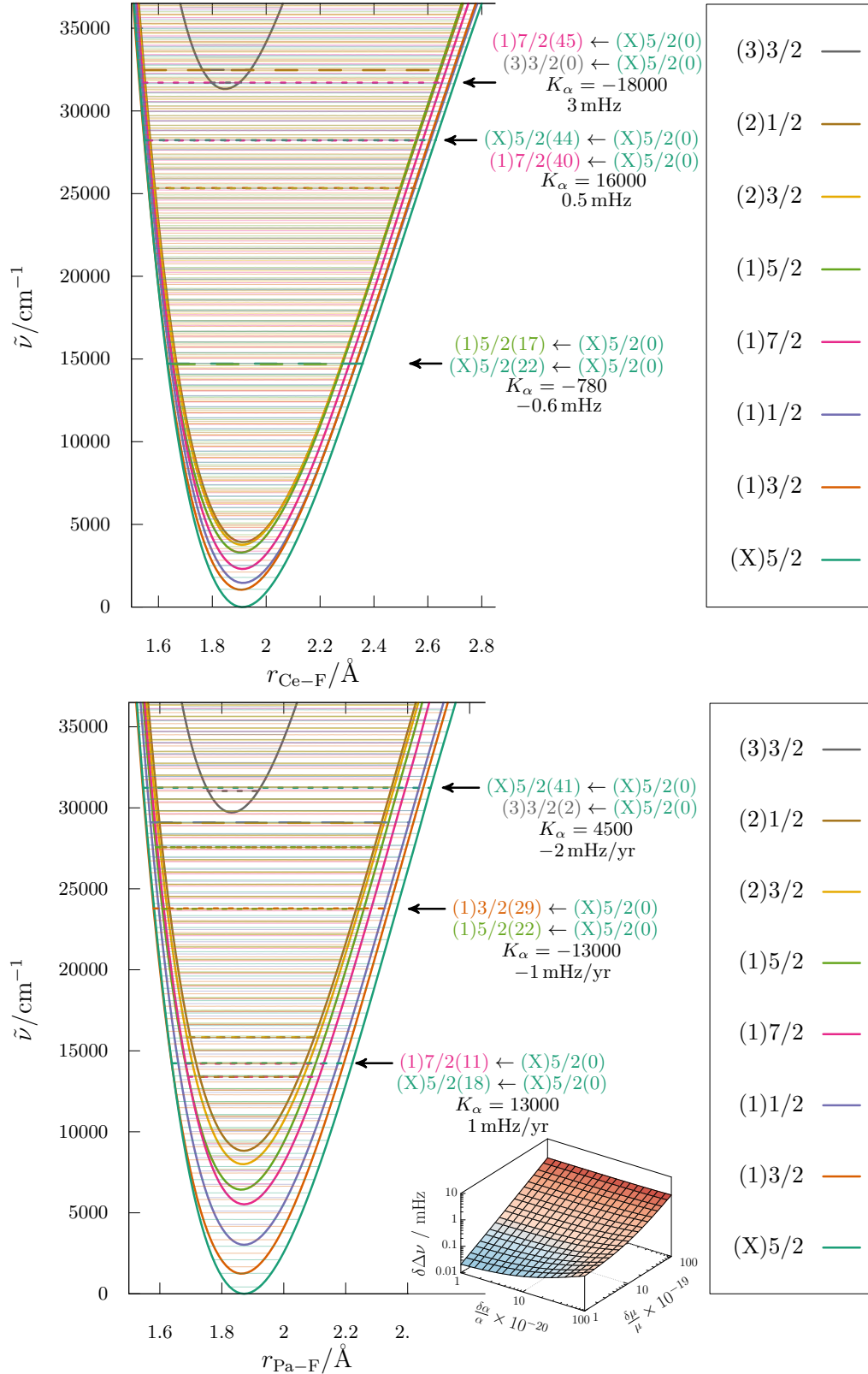


Figure 5. Born-Oppenheimer potential energy curves for CeF^{2+} (top) and PaF^{3+} (bottom, [20]) computed on the level of ZORA-cGHF shown with the respective vibrational energy levels obtained herein with a DVR approach. For CeF^{2+} , we emphasise the similarity to the potential energy curves reported in Ref. [43] due to a similar basis sets employed (see computational details). Exemplary states with pronounced predicted wavenumber shifts due to a variation of the fine-structure constant and the electron-proton mass-ratio are depicted. The surface plot on the bottom shows the frequency shift between transitions $(1)7/2(11) \leftarrow (X)5/2(0)$ and $(X)5/2(18) \leftarrow (X)5/2(0)$ in PaF^{3+} as function of $\delta\alpha/\alpha$ and $\delta\mu/\mu$, where the α -variation was computed using the respective equilibrium structures.

bers we computed the enhancement factors $K_{\alpha,iv}$, $K_{\mu,iv}$ and the natural line width Γ_{iv} for vibronic transitions iv and expected frequency shifts. We ranked the results with decreasing value for $|\Delta K_{\alpha}|$ and give the corresponding transition pairs in Tab. VI. From this we find very large enhancement factors $|\Delta K_{\alpha}| \gg 1000$ for about ten level pairs. For comparison, the enhancement of the most favourable transition in Yb^+ , which provides current best limits on $\delta\alpha$, is $K = -5.95$ [5]. Comparably large absolute values for the enhancement was found previously in high-lying vibronic states of molecular ions such as I_2^+ [11] but with smaller individual $|\Delta q_1|$ values relative to the electronic excitation energy.

We see large $|\Delta q_1|$ values for transitions into the higher lying (3)3/2 state and, thus, also for $|\Delta K|$ as expected from Tab. III and V. These transitions exhibit large absorption linewidths due to multiple possible transitions into lower states dictating the broadening through the sum in Eq. 36.

The absorption linewidth of transitions into energetically lower lying states are expected to be much smaller as Franck–Condon factors for transitions with different Δv become exceedingly small at the cost of a reduced enhancement $|\Delta K|$.

The present Hartree–Fock approach is not highly accurate, and we further want to note that in this ansatz we only include anharmonicities in the vibrational levels within the DVR approach and consider no geometry dependence due to the variation of α . Thus, we can only hint in this work to the numerous possibilities of close lying levels with very large enhancement factors ΔK_{α} and their corresponding linewidths. But for which transitions precisely those near degeneracies emerge depends sensitively on the detailed alignment of electronic states as well as the shape of the potential energy profiles that determine the vibrational level structure, which requires the use of more demanding higher-level computational methods to be predicted reliably.

Corresponding to our presently chosen model, we provide expected wavenumber shifts employing current best limits on $\delta\mu/\mu$ and $\delta\alpha/\alpha$ along with estimated linewidth for pairs of vibronic transitions in Tab. VI. Estimation of expected frequency shifts are obtained as (exemplarily shown for the transition pair (1)7/2(40), (X)5/2(44))

$$\begin{aligned} \delta\Delta\tilde{\nu} &< 0.26 \text{ cm}^{-1} \\ &\times (16000 \times 10^{-18} \text{ yr} + 4500 \times 10^{-17} \text{ yr}) \\ &< 2 \times 10^{-14} \text{ cm}^{-1}/\text{yr} = 0.5 \text{ mHz } c^{-1}/\text{yr}, \end{aligned}$$

where we assume the current best limits for α and μ : $\delta\mu/\mu < 10^{-17} \text{ yr}$ and $\delta\alpha/\alpha < 10^{-18} \text{ yr}$. This relative wavenumber shift on the order of 10^{-14} is in principle measurable with modern high-precision molecular spectroscopy. However, even much larger absolute enhancements may be possible depending on the exact energetic position of the vibronic states which is currently only

crudely described on the HF level. Therefore, we anticipate that high-precision spectroscopy has the potential to improve current bounds on VFC in the near future. We summarize these results in Fig. 5 and conclude that CeF^{2+} can be considered a promising candidate for future precision experiments that aim to detect VFC.

2. PaF^{3+}

The enhancement Δq_1 and Δq_2 of α variations in PaF^{3+} is given in Tab. V. As for CeF^{2+} we show the 40 vibronic transitions with largest absolute enhancement factors ΔK_{α} alongside the linewidth and expected frequency shifts in Tab. VII). From the data in Tab. VII a wide variety of states with different transition wavenumbers and with large absolute sensitivity parameters is observed. An exemplary estimation of the expected frequency shift for the transition pair (1)7/2(11), (X)5/2(18) is given as

$$\begin{aligned} \delta\Delta\tilde{\nu} &< 0.49 \text{ cm}^{-1} \\ &\times (13000 \times 10^{-18} \text{ yr} + 5600 \times 10^{-17} \text{ yr}) \\ &< 3.4 \times 10^{-14} \text{ cm}^{-1}/\text{yr} = 1.0 \text{ mHz } c^{-1}/\text{yr}, \end{aligned}$$

with the same assumptions and limitations to our computational approach as in the case of CeF^{2+} .

PaF^{3+} generally exhibits transitions with larger values for $|\Delta q_1|$ than CeF^{2+} . The transitions with highest absolute sensitivity involve the (3)3/2 state from the ground vibronic state values with (X)5/2 as reference, which is expected from the discussion above.

Computed natural radiative linewidths in PaF^{3+} are similar to those in CeF^{2+} but slightly broader, which aligns with the larger mixing of states with different orbital angular momenta via spin-orbit coupling. Nevertheless, the same arguments (and limitations regarding accuracy of the estimates) as for CeF^{2+} still apply.

Most of the $|\Delta q_1|$ values in PaF^{3+} are larger in magnitude than in CeF^{2+} . Nonetheless, we observe different transition pairs with large absolute shift $\delta\Delta\tilde{\nu}$ in both compounds. This highlights the various possibilities to obtain limits on variations of α and μ at the same time.

V. CONCLUSION

The tedious numerical procedure needed previously to assess the impact of a potential variation of fundamental constants likely hampered routine investigations. We introduced herein an efficient way to compute the sensitivity of atoms and molecules to a variation of the fine-structure constant α via an expectation value of operators that are available in essentially all common *ab initio* relativistic electronic structure programs. By comparison to the conventional numerical approach we demonstrated the advantages of our analytic scheme of computation,

which allows to routinely estimate sensitivities to a variation of α .

As the corresponding expectation values can possibly be found reported in legacy outputs of previous calculations, this approach has the potential to open up access to a rich source of valuable data.

We applied our scheme herein to find huge enhancements of variations of α in the highly charged molecules PaF^{3+} and CeF^{2+} . Both systems are expected to be well-controllable and possess energetically close-lying electronic states of different symmetry, by which many accidentally degenerate vibronic levels emerge that display also large enhancements of changes in α . This highlights that stable polar highly charged molecular ions such as PaF^{3+} or CeF^{2+} are well posed for searches for a tempo-

ral variation of fundamental constants.

ACKNOWLEDGMENTS

We thank Jürgen Stohner and Stephan Malbrunot-Ettenauer for discussions. For the computational work, we acknowledge computing time provided at the NHR Center NHR@SW at Goethe-University Frankfurt. This was funded by the Federal Ministry of Education and Research and the state governments participating on the basis of the resolutions of the GWK for national high performance computing at universities (<http://www.nhr-verein.de/unsere-partner>). C.Z. and R.B. acknowledge funding received from the Deutsche Forschungsgemeinschaft (DFG, German Research Foundation) – Projekt-nummer 445296313.

-
- [1] Jean-Philippe Uzan, “The fundamental constants and their variation: observational and theoretical status,” *Rev. Mod. Phys.* **75**, 403–455 (2003).
- [2] R. M. Godun, P. B. R. Nisbet-Jones, J. M. Jones, S. A. King, L. A. M. Johnson, H. S. Margolis, K. Szymaniec, S. N. Lea, K. Bongs, and P. Gill, “Frequency ratio of two optical clock transitions in $^{171}\text{Yb}^+$ and constraints on the time variation of fundamental constants,” *Phys. Rev. Lett.* **113**, 210801 (2014).
- [3] N. Huntemann, B. Lipphardt, Chr. Tamm, V. Gerginov, S. Weyers, and E. Peik, “Improved limit on a temporal variation of m_p/m_e from comparisons of Yb^+ and Cs atomic clocks,” *Phys. Rev. Lett.* **113**, 210802 (2014).
- [4] R. Lange, N. Huntemann, J. M. Rahm, C. Sanner, H. Shao, B. Lipphardt, Chr. Tamm, S. Weyers, and E. Peik, “Improved limits for violations of local position invariance from atomic clock comparisons,” *Phys. Rev. Lett.* **126**, 011102 (2021).
- [5] Marianna S. Safronova, Sergey G. Porsev, Christian Sanner, and Jun Ye, “Two clock transitions in neutral Yb for the highest sensitivity to variations of the fine-structure constant,” *Phys. Rev. Lett.* **120**, 173001 (2018).
- [6] V. V. Flambaum and M. G. Kozlov, “Enhanced sensitivity to the time variation of the fine-structure constant and m_p/m_e in diatomic molecules,” *Phys. Rev. Lett.* **99**, 150801 (2007).
- [7] D. DeMille, S. B. Cahn, D. Murphree, D. A. Rahmlow, and M. G. Kozlov, “Using molecules to measure nuclear spin-dependent parity violation,” *Phys. Rev. Lett.* **100**, 023003 (2008).
- [8] K. Beloy, A. Borschevsky, P. Schwerdtfeger, and V. V. Flambaum, “Enhanced sensitivity to the time variation of the fine-structure constant and m_p/m_e in diatomic molecules: A closer examination of silicon monobromide,” *Phys. Rev. A* **82**, 022106 (2010).
- [9] K. Beloy, A. Borschevsky, V. V. Flambaum, and P. Schwerdtfeger, “Effect of α variation on a prospective experiment to detect variation of m_e/m_p in diatomic molecules,” *Phys. Rev. A* **84**, 042117 (2011).
- [10] K. Beloy, A. W. Hauser, A. Borschevsky, V. V. Flambaum, and P. Schwerdtfeger, “Effect of α variation on the vibrational spectrum of Sr_2 ,” *Phys. Rev. A* **84**, 062114 (2011).
- [11] L. F. Pařteka, A. Borschevsky, V. V. Flambaum, and P. Schwerdtfeger, “Search for the variation of fundamental constants: Strong enhancements in $X\ ^2\Pi$ cations of dihalogens and hydrogen halides,” *Phys. Rev. A* **92**, 012103 (2015).
- [12] J. C. Berengut, V. A. Dzuba, and V. V. Flambaum, “Enhanced laboratory sensitivity to variation of the fine-structure constant using highly charged ions,” *Phys. Rev. Lett.* **105**, 120801 (2010).
- [13] J. C. Berengut, V. A. Dzuba, V. V. Flambaum, and A. Ong, “Electron-hole transitions in multiply charged ions for precision laser spectroscopy and searching for variations in α ,” *Phys. Rev. Lett.* **106**, 210802 (2011).
- [14] V. A. Dzuba, V. V. Flambaum, and J. K. Webb, “Calculations of the relativistic effects in many-electron atoms and space-time variation of fundamental constants,” *Phys. Rev. A* **59**, 230–237 (1999).
- [15] V. V. Flambaum, “Enhanced effect of temporal variation of the fine-structure constant in diatomic molecules,” *Phys. Rev. A* **73**, 034101 (2006).
- [16] V. V. Flambaum, Y. V. Stadnik, M. G. Kozlov, and A. N. Petrov, “Enhanced effects of temporal variation of the fundamental constants in $^2\Pi_{1/2}$ -term diatomic molecules: $^{207}\text{Pb}^{19}\text{F}$,” *Phys. Rev. A* **88**, 052124 (2013).
- [17] Marianna S. Safronova, “The search for variation of fundamental constants with clocks,” *Annalen der Physik* **531**, 1800364 (2019).
- [18] V. V. Flambaum and M. G. Kozlov, “Studying variation of fundamental constants with molecules,” (2008), [arXiv:0711.4536](https://arxiv.org/abs/0711.4536) [physics.atom-ph].
- [19] DIRAC, a relativistic ab initio electronic structure program, Release DIRAC19 (2019), written by A. S. P. Gomes, T. Saue, L. Visscher, H. J. Aa. Jensen, and R. Bast, with contributions from I. A. Aucar, V. Bakken, K. G. Dyall, S. Dubillard, U. Ekström, E. Eliav, T. Enevoldsen, E. Faßhauer, T. Fleig, O. Fossgaard, L. Halbert, E. D. Hedegård, B. Heimlich–Paris, T. Helgaker, J. Henriksson, M. Iliaş, Ch. R. Jacob,

- S. Knecht, S. Komorovský, O. Kullie, J. K. Lærdahl, C. V. Larsen, Y. S. Lee, H. S. Nataraj, M. K. Nayak, P. Norman, G. Olejniczak, J. Olsen, J. M. H. Olsen, Y. C. Park, J. K. Pedersen, M. Pernpointner, R. di Remigio, K. Ruud, P. Salek, B. Schimmelpfennig, B. Senjean, A. Shee, J. Sikkema, A. J. Thorvaldsen, J. Thyssen, J. van Stralen, M. L. Vidal, S. Villaume, O. Visser, T. Winther, and S. Yamamoto (available at <http://dx.doi.org/10.5281/zenodo.3572669>, see also <http://www.diracprogram.org>).
- [20] Carsten Zülch, Konstantin Gaul, Steffen M. Giesen, Ronald F. Garcia Ruiz, and Robert Berger, “Cool molecular highly charged ions for precision tests of fundamental physics,” arXiv **physics.chem-ph**, 2203.10333 (2022).
- [21] Carsten Zülch, Konstantin Gaul, and Robert Berger, “Fundamental physics with the thermodynamically stable diatomic trication UF^{3+} ,” *Isr. J. Chem.* **63**, e202300035 (2023).
- [22] John K. Webb, Victor V. Flambaum, Christopher W. Churchill, Michael J. Drinkwater, and John D. Barrow, “Search for time variation of the fine structure constant,” *Phys. Rev. Lett.* **82**, 884–887 (1999).
- [23] Anna-Katharina Hansmann and Robert Berger, “Variation of the fine-structure constant in model systems for singlet fission,” *J. Phys. Chem. A* **124**, 6682–6687 (2020), pMID: 32786664, <https://doi.org/10.1021/acs.jpca.0c04685>.
- [24] Kjell Janke, Andrés Emilio Wedenig, Peter Schwerdtfeger, Konstantin Gaul, and Robert Berger, “Quantum electrodynamic corrections for molecules: Vacuum polarization and electron self-energy in a two-component relativistic framework,” *J. Chem. Phys.* **162**, 104111 (2025).
- [25] C. van Wüllen, “Molecular density functional calculations in the regular relativistic approximation: Method, application to coinage metal diatomics, hydrides, fluorides and chlorides, and comparison with first-order relativistic calculations,” *J. Chem. Phys.* **109**, 392–399 (1998).
- [26] Gustavo A. Aucar, Juan I. Melo, Ignacio Agustín Aucar, and Alejandro F. Maldonado, “Foundations of the LRESC model for response properties and some applications,” *Int. J. Quantum Chem.* **118**, e25487 (2018).
- [27] R. Berger, N. Langermann, and C. van Wüllen, “Zeroth order regular approximation approach to molecular parity violation,” *Phys. Rev. A* **71**, 042105 (2005).
- [28] Sophie Nahrwold and Robert Berger, “Zeroth order regular approximation approach to parity violating nuclear magnetic resonance shielding tensors,” *J. Chem. Phys.* **130**, 214101 (2009).
- [29] T. A. Isaev and R. Berger, “Electron correlation and nuclear charge dependence of parity-violating properties in open-shell diatomic molecules,” *Phys. Rev. A* **86**, 062515 (2012).
- [30] Konstantin Gaul and Robert Berger, “Toolbox approach for quasi-relativistic calculation of molecular properties for precision tests of fundamental physics,” *J. Chem. Phys.* **152**, 044101 (2020), arXiv:1907.10432 [physics.chem-ph].
- [31] Sascha A. Brück, Nityananda Sahu, Konstantin Gaul, and Robert Berger, “Quasi-relativistic approach to analytical gradients of parity violating potentials,” *J. Chem. Phys.* **158**, 194109 (2023).
- [32] Mariano T. Colombo Jofré, Karol Koziol, I. Agustín Aucar, Konstantin Gaul, Robert Berger, and Gustavo A. Aucar, “Relativistic and QED corrections to one-bond indirect nuclear spin–spin couplings in X_2^{2+} and X_3^{2+} ions ($X = \text{Zn}, \text{Cd}, \text{Hg}$),” *J. Chem. Phys.* **157**, 064103 (2022), <https://doi.org/10.1063/5.0095586>.
- [33] Christoph van Wüllen, “A Quasirelativistic Two-component Density Functional and Hartree–Fock Program,” *Z. Phys. Chem* **224**, 413–426 (2010).
- [34] R. Ahlrichs, M. Bär, M. Häser, H. Horn, and C. Kölmel, “Electronic structure calculations on workstation computers: The program system turbomole,” *Chem. Phys. Lett.* **162**, 165–169 (1989).
- [35] Wenjian Liu and Christoph van Wüllen, “Spectroscopic constants of gold and eka-gold (element 111) diatomic compounds: The importance of spin–orbit coupling,” *J. Chem. Phys.* **110**, 3730–3735 (1999), https://pubs.aip.org/aip/jcp/article-pdf/110/8/3730/19256335/3730_1_online.pdf.
- [36] Andrew T. B. Gilbert, Nicholas A. Besley, and Peter M. W. Gill, “Self-consistent field calculations of excited states using the maximum overlap method (MOM),” *J. Phys. Chem. A* **112**, 13164–13171 (2008), pMID: 18729344, <https://doi.org/10.1021/jp801738f>.
- [37] Giuseppe M. J. Barca, Andrew T. B. Gilbert, and Peter M. W. Gill, “Simple models for difficult electronic excitations,” *J. Chem. Theo. Comp.* **14**, 1501–1509 (2018), pMID: 29444408, <https://doi.org/10.1021/acs.jctc.7b00994>.
- [38] Per-Olov Löwdin, “Quantum theory of many-particle systems .I. physical interpretations by means of density matrices, natural spin-orbitals, and convergence problems in the method of configurational interaction,” *Phys. Rev.* **97**, 1474–1489 (1955).
- [39] M. Klues, P. Jerabek, T. Breuer, M. Oehzelt, K. Hermann, R. Berger, and G. Witte, “Understanding the F 1s NEXAFS dichroism in fluorinated organic semiconductors,” *J. Chem. Phys. C* **120**, 12693–12705 (2016).
- [40] A. S. P. Gomes, K. G. Dyall, and L. Visscher, “Relativistic double-zeta, triple-zeta, and quadruple-zeta basis sets for the lanthanides la–lu,” *Theor. Chem. Acc.* **127**, 369–381 (2010).
- [41] Kenneth G. Dyall, “Relativistic and nonrelativistic finite nucleus optimized triple-zeta basis sets for the 4p, 5p and 6p elements,” *Theor. Chem. Acc.* **108**, 335–340 (2002).
- [42] Kenneth G. Dyall, “Relativistic quadruple-zeta and revised triple-zeta and double-zeta basis sets for the 4p, 5p, and 6p elements,” *Theor. Chem. Acc.* **115**, 441–447 (2006).
- [43] R. Simpson, C. Zülch, K. B. Ng, I. Belosevic, C. Charles, P. Justus, R. Berger, S. Malbrunot-Ettenauer, A. A. Kwiatkowski, M. P. Reiter, J. Ash, C. Babcock, J. Bergmann, E. Brisley, J. Cardona, C. Chambers, A. Czihaly, A. Gottberg, S. Kakkar, J. Lassen, F. Maldonado Milán, A. Mollaebrahimi, V. Radchenko, E. Taylor, A. Teigelhöfer, C. Walls, A. Weaver, and P. Weligampola, “Formation of gaseous, doubly charged cerium monofluoride CeF^{2+} and its sensitivity to new physics,” to be published.
- [44] “See supplemental material at [url from publisher] for numerical data used in various figures and tables, as well as, raw data obtained from the outputs of the calculatons.”.
- [45] Björn O. Roos, Roland Lindh, Per-Åke Malmqvist, Valera Veryazov, and Per Olof Widmark, “Main Group Atoms and Dimers Studied with a New Relativistic ANO Basis Set,” *J. Phys. Chem. A* **108**, 2851–2858 (2004).

- [46] L. Visscher and K.G. Dyall, “Dirac–fock atomic electronic structure calculations using different nuclear charge distributions,” *At. Data Nucl. Data Tables* **67**, 207–224 (1997).
- [47] Thomas Williams, Colin Kelley, and many others, “Gnuplot 4.6: an interactive plotting program,” <http://gnuplot.sourceforge.net/> (2013).
- [48] R. Meyer, “Trigonometric interpolation method for one-dimensional quantum-mechanical problems,” *J. Chem. Phys.* **52**, 2053–2059 (1970).
- [49] S. M. Udrescu, A. J. Brinson, R. F. Garcia Ruiz, K. Gaul, R. Berger, J. Billowes, C. L. Binnersley, M. L. Bissell, A. A. Breier, K. Chrysalidis, T. E. Cocolios, B. S. Cooper, K. T. Flanagan, T. F. Giesen, R. P. de Groote, S. Franchoo, F. P. Gustafsson, T. A. Isaev, A. Koszorus, G. Neyens, H. A. Perrett, C. M. Ricketts, S. Rothe, A. R. Vernon, K. D. A. Wendt, F. Wienholtz, S. G. Wilkins, and X. F. Yang, “Isotope shifts of radium monofluoride molecules,” *Phys. Rev. Lett.* **127**, 033001 (2021), arXiv:2105.10549 [nucl-ex].
- [50] D. DeMille, S. Sainis, J. Sage, T. Bergeman, S. Kotochigova, and E. Tiesinga, “Enhanced sensitivity to variation of m_e/m_p in molecular spectra,” *Phys. Rev. Lett.* **100**, 043202 (2008).
- [51] Y. Y. Jiang, A. D. Ludlow, N. D. Lemke, R. W. Fox, J. A. Sherman, L.-S. Ma, and C. W. Oates, “Making optical atomic clocks more stable with 10-16 level laser stabilization,” *Nat. Photonics* **5**, 158–161 (2011).
- [52] N. Hinkley, J. A. Sherman, N. B. Phillips, M. Schioppo, N. D. Lemke, K. Beloy, M. Pizzocaro, C. W. Oates, and A. D. Ludlow, “An atomic clock with 10^{-18} instability,” *Science* **341**, 1215–1218 (2013).
- [53] V. A. Dzuba, V. V. Flambaum, and S. Schiller, “Testing physics beyond the standard model through additional clock transitions in neutral ytterbium,” *Phys. Rev. A* **98**, 022501 (2018).
- [54] Th. Udem, R. Holzwarth, and T. W. Hänsch, “Optical frequency metrology,” *Nature* **416**, 233–237 (2002).

Table VI. Accidentally nearly degenerate vibronic transitions pairs with transition wavenumber difference $\Delta\tilde{\nu}$ in CeF^{2+} computed on the level of ZORA-cGFH are shown. The results are ranked according to the enhancement factor ΔK_α . Corresponding electronic sensitivity factors $\Delta\Delta q_1$, enhancement factors ΔK_μ for the variation of the electron-proton mass-ratio, the natural radiative linewidths Γ of the pair of transitions and expected frequency shifts $\delta\Delta\nu$ including the individual contributions from $\delta\alpha$ and $\delta\mu$ are provided. Expected frequency shifts were computed assuming the currently best limits on $\delta\alpha$ and $\delta\mu$ [2-4]: $\delta\mu/\mu < 10^{-17}$ yr and $\delta\alpha/\alpha < 10^{-18}$ yr. The values in parentheses after the term symbol indicate the vibrational quantum number.

| Transition A | Transition B | $\Delta\tilde{\nu}/\text{cm}^{-1}$ | $\Delta\Delta q_1/\text{cm}^{-1}$ | ΔK_α | ΔK_μ | Γ^A/Hz | Γ^B/Hz | $\delta\Delta\nu/\text{mHz}$ | $\delta\Delta\nu_\alpha/\text{mHz}$ | $\delta\Delta\nu_\mu/\text{mHz}$ |
|-----------------|-----------------|------------------------------------|-----------------------------------|--------------------|--------------------|----------------------|----------------------|------------------------------|-------------------------------------|----------------------------------|
| (1)7/2(67) | (3)3/2(16) | 2.5 | 2.6×10^4 | 2.1×10^4 | -5.7×10^3 | 2 | 1×10^7 | -2.80 | 1.55 | -4.4 |
| (3)3/2(11) | (1)7/2(60) | 2.7 | -2.6×10^4 | -1.9×10^4 | 5.5×10^3 | 1×10^7 | 2 | 2.79 | -1.56 | 4.3 |
| (3)3/2(0) | (1)7/2(45) | 2.9 | -2.6×10^4 | -1.8×10^4 | 5.1×10^3 | 2×10^7 | 2 | 2.79 | -1.56 | 4.3 |
| (1)3/2(60) | (3)3/2(9) | 3.0 | 2.4×10^4 | 1.6×10^4 | -5.0×10^3 | 3 | 1×10^7 | -3.10 | 1.44 | -4.5 |
| (1)7/2(40) | (X)5/2(44) | 0.26 | 2.0×10^3 | 1.6×10^4 | 4.5×10^3 | 1 | 4×10^{-4} | 0.47 | 0.12 | 0.35 |
| (1)1/2(37) | (2)3/2(33) | 0.53 | -2.3×10^3 | -8.6×10^3 | -2.2×10^3 | 1 | 4×10^1 | -0.48 | -0.14 | -0.35 |
| (3)3/2(1) | (2)1/2(44) | 12 | -2.6×10^4 | -4.3×10^3 | 1.2×10^3 | 2×10^7 | 2×10^1 | 2.57 | -1.54 | 4.1 |
| (3)3/2(17) | (2)3/2(66) | 13 | -2.6×10^4 | -3.9×10^3 | 1.0×10^3 | 1×10^7 | 3×10^1 | 2.58 | -1.55 | 4.1 |
| (3)3/2(4) | (1)3/2(53) | 13 | -2.4×10^4 | -3.8×10^3 | 1.2×10^3 | 1×10^7 | 3 | 3.10 | -1.44 | 4.5 |
| (1)1/2(61) | (1)5/2(57) | 1.3 | -2.3×10^3 | -3.5×10^3 | -7.0×10^2 | 1 | 6×10^2 | -0.42 | -0.14 | -0.28 |
| (3)3/2(17) | (2)1/2(66) | 16 | -2.6×10^4 | -3.3×10^3 | 8.8×10^2 | 1×10^7 | 2×10^1 | 2.57 | -1.54 | 4.1 |
| (X)5/2(60) | (1)5/2(54) | 1.4 | -2.1×10^3 | -3.0×10^3 | -1.2×10^3 | 7×10^{-4} | 6×10^2 | -0.62 | -0.13 | -0.49 |
| (3)3/2(12) | (2)1/2(59) | 17 | -2.6×10^4 | -3.0×10^3 | 7.9×10^2 | 1×10^7 | 2×10^1 | 2.57 | -1.54 | 4.1 |
| (3)3/2(5) | (X)5/2(56) | 17 | -2.4×10^4 | -2.9×10^3 | 9.4×10^2 | 1×10^7 | 6×10^{-4} | 3.26 | -1.43 | 4.7 |
| (3)3/2(0) | (1)1/2(47) | 17 | -2.4×10^4 | -2.8×10^3 | 8.8×10^2 | 2×10^7 | 1 | 3.05 | -1.42 | 4.5 |
| (1)5/2(57) | (3)3/2(10) | 20 | 2.6×10^4 | 2.7×10^3 | -7.2×10^2 | 6×10^2 | 1×10^7 | -2.64 | 1.56 | -4.2 |
| (1)1/2(61) | (3)3/2(10) | 21 | 2.4×10^4 | 2.3×10^3 | -7.1×10^2 | 1 | 1×10^7 | -3.06 | 1.42 | -4.5 |
| (2)3/2(55) | (3)3/2(9) | 25 | 2.6×10^4 | 2.1×10^3 | -5.5×10^2 | 3×10^1 | 1×10^7 | -2.58 | 1.55 | -4.1 |
| (1)7/2(44) | (1)1/2(46) | 2.6 | 2.3×10^3 | 1.7×10^3 | 1.6×10^2 | 2 | 1 | 0.26 | 0.13 | 0.13 |
| (1)3/2(17) | (1)7/2(15) | 2.3 | -1.9×10^3 | -1.7×10^3 | -2.8×10^2 | 1 | 1 | -0.30 | -0.11 | -0.19 |
| (3)3/2(3) | (1)7/2(49) | 31 | -2.6×10^4 | -1.7×10^3 | 4.6×10^2 | 1×10^7 | 2 | 2.79 | -1.56 | 4.3 |
| (3)3/2(18) | (1)5/2(68) | 34 | -2.6×10^4 | -1.5×10^3 | 4.1×10^2 | 1×10^7 | 6×10^2 | 2.64 | -1.56 | 4.2 |
| (1)1/2(54) | (3)3/2(5) | 31 | 2.4×10^4 | 1.5×10^3 | -4.8×10^2 | 1 | 1×10^7 | -3.06 | 1.42 | -4.5 |
| (3)3/2(10) | (X)5/2(63) | 32 | -2.4×10^4 | -1.5×10^3 | 4.8×10^2 | 1×10^7 | 8×10^{-4} | 3.26 | -1.43 | 4.7 |
| (3)3/2(12) | (2)3/2(59) | 40 | -2.6×10^4 | -1.3×10^3 | 3.5×10^2 | 1×10^7 | 3×10^1 | 2.57 | -1.55 | 4.1 |
| (3)3/2(14) | (1)3/2(67) | 39 | -2.4×10^4 | -1.2×10^3 | 3.9×10^2 | 1×10^7 | 3 | 3.10 | -1.44 | 4.5 |
| (3)3/2(4) | (2)1/2(48) | 44 | -2.6×10^4 | -1.2×10^3 | 3.1×10^2 | 1×10^7 | 2×10^1 | 2.56 | -1.54 | 4.1 |
| (3)3/2(13) | (1)5/2(61) | 49 | -2.6×10^4 | -1.1×10^3 | 2.8×10^2 | 1×10^7 | 6×10^2 | 2.63 | -1.56 | 4.2 |
| (X)5/2(66) | (3)3/2(12) | 47 | 2.4×10^4 | 1.0×10^3 | -3.3×10^2 | 9×10^{-4} | 1×10^7 | -3.27 | 1.43 | -4.7 |
| (3)3/2(15) | (1)1/2(68) | 48 | -2.4×10^4 | -1.0×10^3 | 3.1×10^2 | 1×10^7 | 1 | 3.05 | -1.42 | 4.5 |
| (3)3/2(2) | (1)5/2(46) | 55 | -2.6×10^4 | -9.4×10^2 | 2.5×10^2 | 1×10^7 | 6×10^2 | 2.63 | -1.56 | 4.2 |
| (2)1/2(55) | (3)3/2(9) | 56 | 2.6×10^4 | 9.1×10^2 | -2.4×10^2 | 2×10^1 | 1×10^7 | -2.58 | 1.54 | -4.1 |
| (2)1/2(51) | (1)3/2(56) | 3.7 | 1.6×10^3 | 8.9×10^2 | 3.9×10^2 | 2×10^1 | 3 | 0.53 | 0.10 | 0.43 |
| (2)1/2(25) | (X)5/2(31) | 3.9 | 1.7×10^3 | 8.9×10^2 | 5.0×10^2 | 2×10^1 | 2×10^{-4} | 0.69 | 0.10 | 0.59 |
| (3)3/2(1) | (2)3/2(44) | 59 | -2.6×10^4 | -8.9×10^2 | 2.3×10^2 | 2×10^7 | 3×10^1 | 2.57 | -1.56 | 4.1 |
| (1)3/2(12) | (2)3/2(8) | 4.9 | -1.9×10^3 | -8.0×10^2 | -2.8×10^2 | 1 | 4×10^1 | -0.52 | -0.12 | -0.41 |
| (X)5/2(22) | (1)5/2(17) | 5.6 | -2.2×10^3 | -7.8×10^2 | -3.0×10^2 | 1×10^{-4} | 6×10^2 | -0.63 | -0.13 | -0.50 |
| (1)5/2(64) | (3)3/2(15) | 67 | 2.6×10^4 | 7.7×10^2 | -2.1×10^2 | 6×10^2 | 1×10^7 | -2.65 | 1.56 | -4.2 |
| (1)3/2(49) | (3)3/2(1) | 63 | 2.4×10^4 | 7.6×10^2 | -2.4×10^2 | 2 | 2×10^7 | -3.11 | 1.44 | -4.5 |
| (3)3/2(0) | (X)5/2(49) | 64 | -2.4×10^4 | -7.4×10^2 | 2.4×10^2 | 2×10^7 | 5×10^{-4} | 3.25 | -1.44 | 4.7 |
| (1)7/2(56) | (3)3/2(8) | 70 | 2.6×10^4 | 7.4×10^2 | -2.1×10^2 | 2 | 1×10^7 | -2.80 | 1.56 | -4.4 |
| (2)1/2(69) | (3)3/2(19) | 70 | 2.6×10^4 | 7.4×10^2 | -2.0×10^2 | 2×10^1 | 1×10^7 | -2.58 | 1.54 | -4.1 |
| (1)1/2(31) | (2)1/2(27) | 5.3 | -2.0×10^3 | -7.3×10^2 | -2.3×10^2 | 1 | 2×10^1 | -0.49 | -0.12 | -0.37 |
| (1)3/2(58) | (2)3/2(53) | 5.3 | -1.9×10^3 | -7.2×10^2 | -2.6×10^2 | 3 | 3×10^1 | -0.52 | -0.12 | -0.41 |
| (1)5/2(53) | (3)3/2(7) | 73 | 2.6×10^4 | 7.2×10^2 | -1.9×10^2 | 6×10^2 | 1×10^7 | -2.65 | 1.56 | -4.2 |
| (3)3/2(6) | (1)7/2(53) | 75 | -2.6×10^4 | -6.9×10^2 | 1.9×10^2 | 1×10^7 | 2 | 2.78 | -1.56 | 4.3 |
| (2)3/2(51) | (3)3/2(6) | 76 | 2.6×10^4 | 6.8×10^2 | -1.8×10^2 | 3×10^1 | 1×10^7 | -2.59 | 1.56 | -4.1 |
| (2)3/2(31) | (X)5/2(37) | 6.1 | 2.0×10^3 | 6.8×10^2 | 3.1×10^2 | 4×10^1 | 3×10^{-4} | 0.69 | 0.12 | 0.56 |
| (1)1/2(22) | (1)5/2(19) | 7.3 | -2.4×10^3 | -6.6×10^2 | -1.3×10^2 | 1 | 6×10^2 | -0.42 | -0.14 | -0.28 |
| (3)3/2(8) | (1)1/2(58) | 73 | -2.4×10^4 | -6.5×10^2 | 2.0×10^2 | 1×10^7 | 1 | 3.04 | -1.42 | 4.5 |
| (2)3/2(69) | (3)3/2(19) | 80 | 2.6×10^4 | 6.5×10^2 | -1.7×10^2 | 3×10^1 | 1×10^7 | -2.59 | 1.55 | -4.1 |
| (1)5/2(20) | (1)1/2(23) | 7.4 | 2.4×10^3 | 6.4×10^2 | 1.2×10^2 | 6×10^2 | 1 | 0.42 | 0.14 | 0.27 |
| (X)5/2(52) | (3)3/2(2) | 75 | 2.4×10^4 | 6.4×10^2 | -2.1×10^2 | 6×10^{-4} | 1×10^7 | -3.27 | 1.43 | -4.7 |
| (3)3/2(4) | (2)3/2(48) | 82 | -2.6×10^4 | -6.3×10^2 | 1.7×10^2 | 1×10^7 | 3×10^1 | 2.56 | -1.56 | 4.1 |
| (2)3/2(62) | (3)3/2(14) | 82 | 2.6×10^4 | 6.3×10^2 | -1.7×10^2 | 3×10^1 | 1×10^7 | -2.59 | 1.55 | -4.1 |
| (3)3/2(5) | (1)5/2(50) | 85 | -2.6×10^4 | -6.1×10^2 | 1.6×10^2 | 1×10^7 | 6×10^2 | 2.63 | -1.56 | 4.2 |

Table VII. Accidentally nearly degenerate vibronic transitions pairs with transition wavenumber difference $\Delta\tilde{\nu}$ in PaF^{3+} computed on the level of ZORA-cGHF are shown. The results are ranked according to the enhancement factor ΔK_α . Corresponding electronic sensitivity factors $\Delta\Delta q_1$, enhancement factors ΔK_μ for the variation of the electron-proton mass-ratio, the natural radiative linewidths Γ of the pair of transitions and expected frequency shifts $\delta\Delta\nu$ including the individual contributions from $\delta\alpha$ and $\delta\mu$ are provided. Expected frequency shifts were computed assuming the currently best limits on $\delta\alpha$ and $\delta\mu$ [2-4]: $\delta\mu/\mu < 10^{-17}$ yr and $\delta\alpha/\alpha < 10^{-18}$ yr. The values in parentheses after the term symbol indicate the vibrational quantum number.

| Transition | | $\Delta\tilde{\nu}/\text{cm}^{-1}$ | $\Delta\Delta q_1/\text{cm}^{-1}$ | ΔK_α | ΔK_μ | Γ^A/Hz | Γ^B/Hz | $\delta\Delta\nu/\text{mHz}$ | $\delta\Delta\nu_\alpha/\text{mHz}$ | $\delta\Delta\nu_\mu/\text{mHz}$ |
|------------|------------|------------------------------------|-----------------------------------|--------------------|--------------------|----------------------|----------------------|------------------------------|-------------------------------------|----------------------------------|
| A | B | | | | | | | | | |
| (2)1/2(6) | (1)7/2(10) | 0.059 | -2.8×10^3 | -9.4×10^4 | 2.8×10^4 | 2×10^5 | 6×10^1 | 0.33 | -0.17 | 0.49 |
| (1)7/2(11) | (X)5/2(18) | 0.49 | 3.3×10^3 | 1.3×10^4 | 5.6×10^3 | 6×10^1 | 9×10^{-4} | 1.03 | 0.20 | 0.83 |
| (1)3/2(29) | (1)5/2(22) | 0.57 | -3.6×10^3 | -1.3×10^4 | -4.6×10^3 | 3×10^1 | 1×10^3 | -0.99 | -0.21 | -0.78 |
| (2)1/2(24) | (1)5/2(27) | 0.62 | -3.4×10^3 | -1.1×10^4 | 1.9×10^3 | 2×10^5 | 1×10^3 | 0.16 | -0.20 | 0.36 |
| (2)1/2(8) | (2)3/2(9) | 0.54 | -2.1×10^3 | -7.7×10^3 | 7.6×10^2 | 2×10^5 | 2×10^3 | 0.00 | -0.12 | 0.12 |
| (X)5/2(41) | (3)3/2(2) | 19 | 4.3×10^4 | 4.5×10^3 | -7.9×10^2 | 4×10^{-12} | 4×10^7 | -1.90 | 2.55 | -4.5 |
| (1)1/2(34) | (2)1/2(26) | 1.5 | -2.9×10^3 | -3.8×10^3 | -1.9×10^3 | 2×10^2 | 2×10^5 | -1.04 | -0.17 | -0.87 |
| (3)3/2(3) | (2)1/2(30) | 25 | -4.3×10^4 | -3.5×10^3 | 4.2×10^2 | 4×10^7 | 2×10^5 | 0.53 | -2.60 | 3.1 |
| (3)3/2(6) | (X)5/2(46) | 25 | -4.2×10^4 | -3.4×10^3 | 5.9×10^2 | 4×10^7 | 2×10^{-10} | 1.90 | -2.55 | 4.5 |
| (1)5/2(26) | (2)1/2(23) | 2.1 | 3.4×10^3 | 3.3×10^3 | -5.7×10^2 | 1×10^3 | 2×10^5 | -0.15 | 0.21 | -0.36 |
| (2)3/2(8) | (2)1/2(7) | 1.3 | 2.1×10^3 | 3.2×10^3 | -3.1×10^2 | 2×10^3 | 2×10^5 | 0.00 | 0.13 | -0.12 |
| (3)3/2(3) | (1)5/2(33) | 38 | -4.7×10^4 | -2.4×10^3 | 3.0×10^2 | 4×10^7 | 1×10^3 | 0.69 | -2.79 | 3.5 |
| (2)1/2(25) | (1)5/2(28) | 3.0 | -3.4×10^3 | -2.2×10^3 | 3.9×10^2 | 2×10^5 | 1×10^3 | 0.16 | -0.20 | 0.36 |
| (1)1/2(34) | (1)5/2(29) | 6.7 | -6.3×10^3 | -1.9×10^3 | -2.5×10^2 | 2×10^2 | 1×10^3 | -0.89 | -0.38 | -0.51 |
| (2)1/2(9) | (2)3/2(10) | 2.4 | -2.1×10^3 | -1.7×10^3 | 1.7×10^2 | 2×10^5 | 2×10^3 | 0.00 | -0.12 | 0.12 |
| (3)3/2(3) | (2)3/2(31) | 67 | -4.5×10^4 | -1.4×10^3 | 1.6×10^2 | 4×10^7 | 2×10^3 | 0.54 | -2.71 | 3.2 |
| (1)5/2(25) | (2)1/2(22) | 5.1 | 3.4×10^3 | 1.3×10^3 | -2.3×10^2 | 1×10^3 | 2×10^5 | -0.15 | 0.21 | -0.36 |
| (1)7/2(32) | (3)3/2(1) | 68 | 4.6×10^4 | 1.3×10^3 | -1.8×10^2 | 6×10^1 | 5×10^7 | -0.89 | 2.75 | -3.6 |
| (2)1/2(26) | (1)5/2(29) | 5.2 | -3.4×10^3 | -1.3×10^3 | 2.3×10^2 | 2×10^5 | 1×10^3 | 0.16 | -0.20 | 0.36 |
| (2)3/2(7) | (2)1/2(6) | 3.2 | 2.1×10^3 | 1.3×10^3 | -1.3×10^2 | 2×10^3 | 2×10^5 | 0.00 | 0.13 | -0.12 |
| (2)3/2(30) | (3)3/2(2) | 77 | 4.5×10^4 | 1.2×10^3 | -1.4×10^2 | 2×10^3 | 4×10^7 | -0.56 | 2.71 | -3.3 |
| (3)3/2(2) | (1)7/2(33) | 84 | -4.6×10^4 | -1.1×10^3 | 1.4×10^2 | 4×10^7 | 6×10^1 | 0.87 | -2.75 | 3.6 |
| (1)7/2(0) | (1)1/2(3) | 11 | 5.5×10^3 | 1.0×10^3 | 1.2×10^2 | 1×10^2 | 2×10^2 | 0.70 | 0.33 | 0.37 |
| (1)5/2(7) | (X)5/2(15) | 8.6 | 4.3×10^3 | 1.0×10^3 | 3.7×10^2 | 1×10^3 | 6×10^{-4} | 1.22 | 0.26 | 0.96 |
| (2)1/2(10) | (2)3/2(11) | 4.3 | -2.1×10^3 | -9.7×10^2 | 9.6×10^1 | 2×10^5 | 2×10^3 | 0.00 | -0.12 | 0.12 |
| (2)1/2(27) | (1)5/2(30) | 7.1 | -3.4×10^3 | -9.4×10^2 | 1.7×10^2 | 2×10^5 | 1×10^3 | 0.16 | -0.20 | 0.36 |
| (1)5/2(32) | (3)3/2(2) | 110 | 4.7×10^4 | 8.8×10^2 | -1.1×10^2 | 1×10^3 | 4×10^7 | -0.71 | 2.79 | -3.5 |
| (1)5/2(24) | (2)1/2(21) | 8.5 | 3.5×10^3 | 8.2×10^2 | -1.4×10^2 | 1×10^3 | 2×10^5 | -0.15 | 0.21 | -0.36 |
| (2)3/2(6) | (2)1/2(5) | 5.1 | 2.1×10^3 | 8.2×10^2 | -8.1×10^1 | 2×10^3 | 2×10^5 | 0.00 | 0.13 | -0.12 |
| (2)1/2(29) | (3)3/2(2) | 120 | 4.3×10^4 | 7.4×10^2 | -9.0×10^1 | 2×10^5 | 4×10^7 | -0.55 | 2.60 | -3.1 |
| (2)1/2(28) | (1)5/2(31) | 9.0 | -3.3×10^3 | -7.4×10^2 | 1.3×10^2 | 2×10^5 | 1×10^3 | 0.16 | -0.20 | 0.36 |
| (2)1/2(11) | (2)3/2(12) | 6.1 | -2.0×10^3 | -6.7×10^2 | 6.7×10^1 | 2×10^5 | 2×10^3 | 0.00 | -0.12 | 0.12 |
| (1)7/2(9) | (2)1/2(5) | 8.5 | 2.8×10^3 | 6.5×10^2 | -2.0×10^2 | 6×10^1 | 2×10^5 | -0.33 | 0.17 | -0.50 |
| (1)3/2(30) | (2)3/2(21) | 6.3 | -2.0×10^3 | -6.5×10^2 | -5.4×10^2 | 3×10^1 | 2×10^3 | -1.14 | -0.12 | -1.0 |
| (2)1/2(7) | (1)7/2(11) | 8.6 | -2.8×10^3 | -6.4×10^2 | 1.9×10^2 | 2×10^5 | 6×10^1 | 0.33 | -0.17 | 0.49 |
| (2)3/2(5) | (2)1/2(4) | 7.0 | 2.1×10^3 | 6.0×10^2 | -5.9×10^1 | 2×10^3 | 2×10^5 | 0.00 | 0.13 | -0.12 |
| (2)1/2(29) | (1)5/2(32) | 11 | -3.3×10^3 | -6.0×10^2 | 1.1×10^2 | 2×10^5 | 1×10^3 | 0.16 | -0.20 | 0.36 |
| (1)5/2(23) | (2)1/2(20) | 12 | 3.5×10^3 | 5.8×10^2 | -1.0×10^2 | 1×10^3 | 2×10^5 | -0.15 | 0.21 | -0.36 |
| (1)3/2(34) | (1)7/2(28) | 9.5 | -2.7×10^3 | -5.7×10^2 | -2.3×10^2 | 3×10^1 | 6×10^1 | -0.81 | -0.16 | -0.64 |
| (3)3/2(3) | (X)5/2(42) | 160 | -4.3×10^4 | -5.3×10^2 | 9.2×10^1 | 4×10^7 | 5×10^{-11} | 1.88 | -2.55 | 4.4 |
| (X)5/2(45) | (3)3/2(5) | 160 | 4.3×10^4 | 5.3×10^2 | -9.3×10^1 | 3×10^{-10} | 4×10^7 | -1.93 | 2.55 | -4.5 |
| (3)3/2(4) | (2)1/2(31) | 170 | -4.3×10^4 | -5.2×10^2 | 6.2×10^1 | 4×10^7 | 2×10^5 | 0.51 | -2.60 | 3.1 |
| (2)1/2(12) | (2)3/2(13) | 7.9 | -2.0×10^3 | -5.2×10^2 | 5.2×10^1 | 2×10^5 | 2×10^3 | 0.00 | -0.12 | 0.12 |
| (3)3/2(4) | (1)5/2(34) | 180 | -4.7×10^4 | -5.1×10^2 | 6.3×10^1 | 4×10^7 | 9×10^2 | 0.67 | -2.79 | 3.5 |
| (2)3/2(8) | (X)5/2(18) | 10 | 2.7×10^3 | 5.1×10^2 | 3.8×10^2 | 2×10^3 | 9×10^{-4} | 1.36 | 0.16 | 1.2 |
| (1)5/2(30) | (X)5/2(39) | 17 | 4.0×10^3 | 4.9×10^2 | 1.9×10^2 | 1×10^3 | 1×10^{-4} | 1.20 | 0.24 | 0.96 |
| (2)1/2(30) | (1)5/2(33) | 14 | -3.3×10^3 | -4.9×10^2 | 8.8×10^1 | 2×10^5 | 1×10^3 | 0.16 | -0.20 | 0.36 |
| (2)3/2(4) | (2)1/2(3) | 8.9 | 2.1×10^3 | 4.8×10^2 | -4.7×10^1 | 2×10^3 | 2×10^5 | 0.00 | 0.13 | -0.12 |
| (1)5/2(22) | (2)1/2(19) | 16 | 3.5×10^3 | 4.4×10^2 | -7.5×10^1 | 1×10^3 | 2×10^5 | -0.15 | 0.21 | -0.36 |
| (X)5/2(40) | (3)3/2(1) | 200 | 4.3×10^4 | 4.3×10^2 | -7.6×10^1 | 2×10^{-12} | 5×10^7 | -1.93 | 2.55 | -4.5 |
| (3)3/2(4) | (2)3/2(32) | 210 | -4.5×10^4 | -4.3×10^2 | 5.1×10^1 | 4×10^7 | 2×10^3 | 0.52 | -2.71 | 3.2 |
| (X)5/2(39) | (2)3/2(28) | 12 | -2.6×10^3 | -4.3×10^2 | -3.3×10^2 | 1×10^{-4} | 2×10^3 | -1.36 | -0.15 | -1.2 |
| (X)5/2(14) | (1)5/2(6) | 20 | -4.3×10^3 | -4.3×10^2 | -1.6×10^2 | 5×10^{-4} | 1×10^3 | -1.23 | -0.26 | -0.97 |
| (2)1/2(13) | (2)3/2(14) | 9.6 | -2.0×10^3 | -4.2×10^2 | 4.2×10^1 | 2×10^5 | 2×10^3 | 0.00 | -0.12 | 0.12 |
| (X)5/2(38) | (1)5/2(29) | 19 | -4.1×10^3 | -4.2×10^2 | -1.7×10^2 | 9×10^{-5} | 1×10^3 | -1.21 | -0.24 | -0.97 |
| (2)3/2(0) | (1)1/2(6) | 23 | 4.8×10^3 | 4.2×10^2 | 1.1×10^2 | 3×10^3 | 2×10^2 | 1.03 | 0.29 | 0.74 |

Supplementary Material for: Enhanced sensitivity to variations of fundamental constants in highly charged molecules from analytic perturbation theory

Carsten Zülch,¹ Konstantin Gaul,¹ and Robert Berger^{1,*}

¹*Fachbereich Chemie, Philipps-Universität Marburg, Hans-Meerwein-Straße 4, 35032 Marburg*

(Dated: November 17, 2025)

S1. DESCRIPTION

Herein, we display the potential energy curve of CeF^{2+} at the level of 2c-ZORA-cGHF, and report numerical data used in various figures and tables of the main text. Except for table S4, we give raw data obtained from the outputs of the calculations, which provide more digits than we consider numerically stable (see computational details of the main text).

S2. POTENTIAL ENERGY CURVES

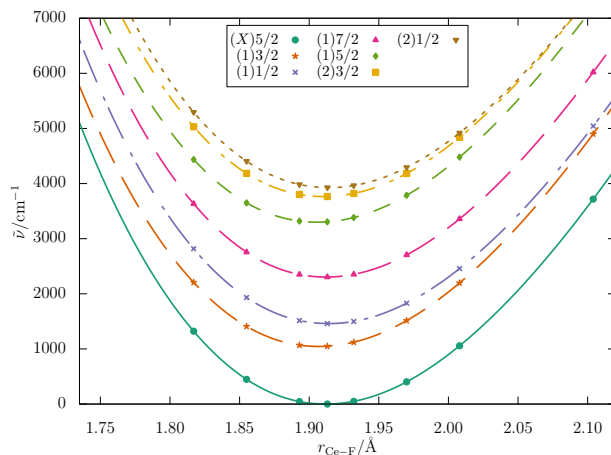


Figure S1. Potential energy curves (at $c = c_0 = 137.0359895 a_0 E_h \hbar^{-1}$) for the seven energetically lowest electronic states relative to the energetic minimum of the electronic ground state of CeF^{2+} computed on the level of ZORA-cGHF.

* robert.berger@uni-marburg.de

S3. TABLES OF NUMERICAL DATA

Table S1. Internuclear distance of CeF^{2+} used as equilibrium bond lengths for each electronic state (at $c = c_0 = 137.0359895 a_0 E_h \hbar^{-1}$) as described in the computational details.

| State | $r_e^{\text{ZORA-cGHF}} / a_0$ | $r_e^{\text{AOC-DHF}} / a_0$ |
|--------|--------------------------------|------------------------------|
| (X)5/2 | 3.613 125 476 387 88 | 3.613 529 811 0 |
| (1)3/2 | 3.603 386 380 929 78 | 3.603 294 844 0 |
| (1)1/2 | 3.616 848 959 330 93 | 3.616 786 838 0 |
| (1)7/2 | 3.613 461 122 658 98 | 3.613 651 684 0 |
| (1)5/2 | 3.601 424 124 826 50 | 3.601 840 339 0 |
| (2)3/2 | 3.610 332 366 423 55 | 3.610 605 330 0 |
| (2)1/2 | 3.617 611 662 836 08 | 3.618 728 385 0 |

Table S2. Total energies of CeF^{2+} (at $c = c_0 = 137.0359895 a_0 E_h \hbar^{-1}$) as a function of the Ce-F internuclear distance calculated on the level of 2c-ZORA-cGHF. Values with '—' only converged to a less than desired criteria and, thus, were not taken into account.

| r/a_0 | (X)5/2 | (1)3/2 | (1)1/2 | E/E_h (1)7/2 | (1)5/2 | (2)3/2 | (2)1/2 |
|----------|---------------------|---------------------|---------------------|---------------------|---------------------|---------------------|---------------------|
| 2.530 05 | -9122.711 438 469 7 | -9122.717 014 168 0 | -9122.699 893 436 8 | -9122.693 514 803 2 | -9122.700 806 341 0 | -9122.692 045 997 5 | -9122.689 100 595 3 |
| 2.710 77 | -9122.892 270 333 0 | -9122.896 594 074 9 | -9122.884 513 451 0 | -9122.879 269 747 2 | -9122.884 512 990 8 | -9122.876 443 719 3 | -9122.873 249 254 7 |
| 2.891 49 | -9123.009 595 116 5 | -9123.011 201 326 2 | -9123.002 801 312 0 | -9122.998 274 292 2 | -9123.000 680 769 0 | -9122.994 286 634 0 | -9122.991 366 083 8 |
| 3.072 21 | -9123.083 755 602 1 | -9123.082 800 553 9 | -9123.076 972 501 5 | -9123.072 938 221 0 | -9123.072 696 565 1 | -9123.067 915 872 6 | -9123.065 548 608 9 |
| 3.252 92 | -9123.127 273 413 7 | -9123.124 462 922 7 | -9123.120 419 857 9 | -9123.116 652 907 1 | -9123.114 388 813 9 | -9123.110 822 426 0 | -9123.109 065 760 8 |
| 3.433 64 | -9123.148 862 014 5 | -9123.144 828 401 0 | -9123.142 044 187 5 | -9123.138 326 799 2 | -9123.134 666 340 1 | -9123.131 959 606 4 | -9123.130 756 654 0 |
| 3.505 93 | -9123.152 842 778 7 | -9123.148 461 395 7 | -9123.146 075 998 3 | -9123.142 325 857 2 | -9123.138 253 540 8 | -9123.135 816 047 1 | -9123.134 809 687 9 |
| 3.578 22 | -9123.154 678 374 5 | -9123.150 015 198 6 | -9123.147 982 498 2 | -9123.144 173 991 0 | -9123.139 759 565 2 | -9123.137 558 493 5 | -9123.136 734 086 1 |
| 3.614 36 | -9123.154 884 033 2 | -9123.150 101 904 0 | -9123.148 230 565 2 | -9123.144 384 204 7 | -9123.139 822 089 3 | -9123.137 728 651 4 | -9123.136 989 921 4 |
| 3.650 50 | -9123.154 660 010 0 | -9123.149 772 171 0 | -9123.148 053 284 8 | -9123.144 163 780 6 | -9123.139 468 137 9 | -9123.137 476 110 1 | -9123.136 819 665 9 |
| 3.722 79 | -9123.153 046 807 4 | -9123.147 983 454 7 | -9123.146 545 537 8 | -9123.142 555 371 3 | -9123.137 631 198 4 | -9123.135 825 473 5 | -9123.135 323 920 3 |
| 3.795 08 | -9123.150 069 239 4 | -9123.144 872 384 1 | -9123.143 687 559 3 | -9123.139 580 007 5 | -9123.134 472 553 5 | -9123.132 834 192 8 | -9123.132 475 499 1 |
| 3.975 80 | -9123.137 941 668 8 | -9123.132 555 147 0 | -9123.131 905 881 5 | -9123.127 450 189 8 | -9123.122 040 867 7 | -9123.120 756 687 2 | -9123.120 709 184 6 |
| 4.156 51 | -9123.121 098 050 7 | -9123.115 667 554 2 | -9123.115 448 441 0 | -9123.110 597 753 2 | -9123.105 046 573 3 | -9123.104 049 145 0 | -9123.104 258 324 3 |
| 4.337 23 | -9123.101 411 028 3 | -9123.096 026 786 7 | -9123.096 160 363 6 | -9123.090 898 805 5 | -9123.085 307 289 0 | -9123.084 548 658 7 | -9123.084 971 138 8 |
| 4.517 95 | -9123.080 202 121 7 | -9123.074 916 815 9 | -9123.075 343 691 3 | -9123.069 676 865 5 | -9123.064 106 741 7 | -9123.063 551 029 5 | -9123.064 151 615 3 |
| 4.698 67 | -9123.058 385 800 7 | -9123.053 227 060 9 | -9123.053 900 163 7 | -9123.047 847 630 1 | -9123.042 333 648 2 | -9123.041 953 398 5 | -9123.042 702 567 5 |
| 4.879 39 | -9123.036 582 949 7 | -9123.031 561 214 7 | -9123.032 442 086 5 | -9123.026 032 972 0 | -9123.020 590 210 3 | -9123.020 365 846 4 | -9123.021 236 593 5 |
| 5.060 10 | -9123.015 215 153 6 | -9123.010 323 384 0 | -9123.011 378 627 8 | -9123.004 657 126 3 | -9122.999 274 453 9 | -9122.999 205 022 4 | -9123.000 161 064 7 |
| 5.240 82 | -9122.994 337 761 5 | -9122.989 646 934 2 | -9122.990 872 988 7 | -9122.983 752 712 2 | -9122.978 638 281 5 | -9122.978 324 839 4 | -9122.979 565 878 0 |
| 5.421 54 | -9122.974 576 785 8 | -9122.969 985 410 4 | -9122.971 325 154 2 | -9122.963 989 470 8 | -9122.958 847 351 6 | -9122.958 878 583 7 | -9122.960 088 271 3 |
| 5.602 26 | -9122.955 663 985 5 | -9122.951 184 642 3 | -9122.952 629 348 7 | -9122.945 070 604 7 | -9122.939 985 890 9 | -9122.940 119 682 0 | -9122.941 375 288 9 |
| 5.782 98 | -9122.937 733 581 4 | -9122.933 358 451 2 | -9122.934 889 835 0 | -9122.927 134 871 0 | -9122.922 103 888 1 | -9122.922 312 721 5 | -9122.923 613 156 2 |
| 5.963 69 | -9122.920 812 558 0 | -9122.916 533 739 1 | -9122.918 132 745 4 | -9122.910 209 885 2 | -9122.905 220 983 6 | -9122.905 490 737 6 | -9122.906 826 050 2 |
| 6.144 41 | -9122.904 905 008 6 | -9122.900 724 238 3 | -9122.902 366 646 6 | -9122.894 299 756 1 | -9122.889 338 340 1 | -9122.889 662 255 4 | -9122.891 018 671 9 |
| 6.325 13 | -9122.890 002 556 4 | -9122.885 990 224 2 | -9122.887 604 486 5 | -9122.879 395 364 6 | -9122.874 446 058 8 | -9122.874 838 013 1 | -9122.876 190 598 9 |
| 6.505 85 | -9122.876 078 556 3 | — | — | -9122.865 478 096 9 | — | -9122.861 182 832 3 | -9122.862 446 147 3 |
| 6.686 57 | -9122.863 129 158 6 | -9122.858 951 918 1 | -9122.860 826 946 6 | -9122.852 526 954 1 | -9122.847 546 595 7 | -9122.847 802 576 1 | -9122.849 298 376 7 |
| 6.867 28 | -9122.851 116 064 9 | -9122.847 071 685 5 | -9122.848 919 143 6 | -9122.840 515 697 2 | -9122.835 494 770 4 | -9122.835 814 662 6 | -9122.837 198 413 5 |
| 7.048 00 | -9122.840 022 332 0 | -9122.836 107 480 0 | -9122.837 946 529 6 | -9122.829 424 429 7 | -9122.824 339 433 6 | -9122.824 684 567 8 | -9122.826 011 420 2 |
| 7.228 72 | -9122.829 850 223 0 | -9122.826 114 800 5 | -9122.827 943 199 6 | -9122.819 254 873 1 | -9122.814 069 000 6 | -9122.814 443 014 3 | -9122.815 676 484 8 |

Table S3. Values of q_1 of individual electronic states in CeF^{2+} as a function of the Ce–F internuclear distance calculated on the level of 2c-ZORA-cGHF (at $c = c_0 = 137.0359895 a_0 E_h \hbar^{-1}$). Values with ‘—’ only converged to a less than desired criteria and, thus, were not taken into account.

| r/a_0 | (X)5/2 | (1)3/2 | (1)1/2 | $hc_0 q_1/E_h$ (1)7/2 | (1)5/2 | (2)3/2 | (2)1/2 |
|----------|-----------------------------|-----------------------------|-----------------------------|-----------------------------|-----------------------------|-----------------------------|-----------------------------|
| 2.530 05 | $-0.511 424 47 \times 10^3$ | $-0.511 428 49 \times 10^3$ | $-0.511 441 52 \times 10^3$ | $-0.511 418 71 \times 10^3$ | $-0.511 423 11 \times 10^3$ | $-0.511 429 49 \times 10^3$ | $-0.511 436 79 \times 10^3$ |
| 2.710 77 | $-0.511 441 83 \times 10^3$ | $-0.511 442 87 \times 10^3$ | $-0.511 451 88 \times 10^3$ | $-0.511 434 18 \times 10^3$ | $-0.511 435 87 \times 10^3$ | $-0.511 440 15 \times 10^3$ | $-0.511 446 98 \times 10^3$ |
| 2.891 49 | $-0.511 455 40 \times 10^3$ | $-0.511 454 60 \times 10^3$ | $-0.511 460 79 \times 10^3$ | $-0.511 446 30 \times 10^3$ | $-0.511 446 18 \times 10^3$ | $-0.511 449 31 \times 10^3$ | $-0.511 454 95 \times 10^3$ |
| 3.072 21 | $-0.511 464 00 \times 10^3$ | $-0.511 463 06 \times 10^3$ | $-0.511 467 35 \times 10^3$ | $-0.511 454 77 \times 10^3$ | $-0.511 454 03 \times 10^3$ | $-0.511 456 11 \times 10^3$ | $-0.511 460 38 \times 10^3$ |
| 3.252 92 | $-0.511 469 48 \times 10^3$ | $-0.511 468 69 \times 10^3$ | $-0.511 471 67 \times 10^3$ | $-0.511 460 26 \times 10^3$ | $-0.511 459 43 \times 10^3$ | $-0.511 460 70 \times 10^3$ | $-0.511 463 77 \times 10^3$ |
| 3.433 64 | $-0.511 472 87 \times 10^3$ | $-0.511 472 26 \times 10^3$ | $-0.511 474 34 \times 10^3$ | $-0.511 463 66 \times 10^3$ | $-0.511 462 91 \times 10^3$ | $-0.511 463 65 \times 10^3$ | $-0.511 465 79 \times 10^3$ |
| 3.505 93 | $-0.511 473 83 \times 10^3$ | $-0.511 473 28 \times 10^3$ | $-0.511 475 08 \times 10^3$ | $-0.511 464 61 \times 10^3$ | $-0.511 463 91 \times 10^3$ | $-0.511 464 50 \times 10^3$ | $-0.511 466 34 \times 10^3$ |
| 3.578 22 | $-0.511 474 62 \times 10^3$ | $-0.511 474 12 \times 10^3$ | $-0.511 475 69 \times 10^3$ | $-0.511 465 40 \times 10^3$ | $-0.511 464 75 \times 10^3$ | $-0.511 465 20 \times 10^3$ | $-0.511 466 79 \times 10^3$ |
| 3.614 36 | $-0.511 474 96 \times 10^3$ | $-0.511 474 49 \times 10^3$ | $-0.511 475 95 \times 10^3$ | $-0.511 465 74 \times 10^3$ | $-0.511 465 11 \times 10^3$ | $-0.511 465 51 \times 10^3$ | $-0.511 466 98 \times 10^3$ |
| 3.650 50 | $-0.511 475 27 \times 10^3$ | $-0.511 474 83 \times 10^3$ | $-0.511 476 18 \times 10^3$ | $-0.511 466 05 \times 10^3$ | $-0.511 465 45 \times 10^3$ | $-0.511 465 79 \times 10^3$ | $-0.511 467 15 \times 10^3$ |
| 3.722 79 | $-0.511 475 81 \times 10^3$ | $-0.511 475 42 \times 10^3$ | $-0.511 476 59 \times 10^3$ | $-0.511 466 58 \times 10^3$ | $-0.511 466 03 \times 10^3$ | $-0.511 466 28 \times 10^3$ | $-0.511 467 45 \times 10^3$ |
| 3.795 08 | $-0.511 476 27 \times 10^3$ | $-0.511 475 92 \times 10^3$ | $-0.511 476 93 \times 10^3$ | $-0.511 467 04 \times 10^3$ | $-0.511 466 52 \times 10^3$ | $-0.511 466 70 \times 10^3$ | $-0.511 467 71 \times 10^3$ |
| 3.975 80 | $-0.511 477 14 \times 10^3$ | $-0.511 476 87 \times 10^3$ | $-0.511 477 56 \times 10^3$ | $-0.511 467 88 \times 10^3$ | $-0.511 467 46 \times 10^3$ | $-0.511 467 49 \times 10^3$ | $-0.511 468 18 \times 10^3$ |
| 4.156 51 | $-0.511 477 74 \times 10^3$ | $-0.511 477 54 \times 10^3$ | $-0.511 477 99 \times 10^3$ | $-0.511 468 47 \times 10^3$ | $-0.511 468 12 \times 10^3$ | $-0.511 468 04 \times 10^3$ | $-0.511 468 52 \times 10^3$ |
| 4.337 23 | $-0.511 478 19 \times 10^3$ | $-0.511 478 02 \times 10^3$ | $-0.511 478 31 \times 10^3$ | $-0.511 468 90 \times 10^3$ | $-0.511 468 60 \times 10^3$ | $-0.511 468 46 \times 10^3$ | $-0.511 468 79 \times 10^3$ |
| 4.517 95 | $-0.511 478 53 \times 10^3$ | $-0.511 478 39 \times 10^3$ | $-0.511 478 56 \times 10^3$ | $-0.511 469 22 \times 10^3$ | $-0.511 468 96 \times 10^3$ | $-0.511 468 78 \times 10^3$ | $-0.511 469 00 \times 10^3$ |
| 4.698 67 | $-0.511 478 79 \times 10^3$ | $-0.511 478 68 \times 10^3$ | $-0.511 478 76 \times 10^3$ | $-0.511 469 46 \times 10^3$ | $-0.511 469 24 \times 10^3$ | $-0.511 469 03 \times 10^3$ | $-0.511 469 18 \times 10^3$ |
| 4.879 39 | $-0.511 478 98 \times 10^3$ | $-0.511 478 89 \times 10^3$ | $-0.511 478 91 \times 10^3$ | $-0.511 469 64 \times 10^3$ | $-0.511 469 46 \times 10^3$ | $-0.511 469 22 \times 10^3$ | $-0.511 469 32 \times 10^3$ |
| 5.060 10 | $-0.511 479 10 \times 10^3$ | $-0.511 479 05 \times 10^3$ | $-0.511 479 02 \times 10^3$ | $-0.511 469 74 \times 10^3$ | $-0.511 469 61 \times 10^3$ | $-0.511 469 33 \times 10^3$ | $-0.511 469 44 \times 10^3$ |
| 5.240 82 | $-0.511 479 01 \times 10^3$ | $-0.511 478 88 \times 10^3$ | $-0.511 478 90 \times 10^3$ | $-0.511 469 63 \times 10^3$ | $-0.511 469 72 \times 10^3$ | $-0.511 469 72 \times 10^3$ | $-0.511 468 89 \times 10^3$ |
| 5.421 54 | $-0.511 479 29 \times 10^3$ | $-0.511 479 22 \times 10^3$ | $-0.511 479 15 \times 10^3$ | $-0.511 469 91 \times 10^3$ | $-0.511 469 78 \times 10^3$ | $-0.511 469 51 \times 10^3$ | $-0.511 469 53 \times 10^3$ |
| 5.602 26 | $-0.511 479 29 \times 10^3$ | $-0.511 479 24 \times 10^3$ | $-0.511 479 16 \times 10^3$ | $-0.511 469 91 \times 10^3$ | $-0.511 469 79 \times 10^3$ | $-0.511 469 55 \times 10^3$ | $-0.511 469 55 \times 10^3$ |
| 5.782 98 | $-0.511 479 23 \times 10^3$ | $-0.511 479 20 \times 10^3$ | $-0.511 479 12 \times 10^3$ | $-0.511 469 84 \times 10^3$ | $-0.511 469 75 \times 10^3$ | $-0.511 469 51 \times 10^3$ | $-0.511 469 50 \times 10^3$ |
| 5.963 69 | $-0.511 479 11 \times 10^3$ | $-0.511 479 10 \times 10^3$ | $-0.511 479 03 \times 10^3$ | $-0.511 469 71 \times 10^3$ | $-0.511 469 64 \times 10^3$ | $-0.511 469 41 \times 10^3$ | $-0.511 469 40 \times 10^3$ |
| 6.144 41 | $-0.511 478 91 \times 10^3$ | $-0.511 478 90 \times 10^3$ | $-0.511 478 87 \times 10^3$ | $-0.511 469 51 \times 10^3$ | $-0.511 469 46 \times 10^3$ | $-0.511 469 23 \times 10^3$ | $-0.511 469 24 \times 10^3$ |
| 6.325 13 | $-0.511 478 63 \times 10^3$ | $-0.511 478 40 \times 10^3$ | $-0.511 478 59 \times 10^3$ | $-0.511 469 23 \times 10^3$ | $-0.511 469 22 \times 10^3$ | $-0.511 468 92 \times 10^3$ | $-0.511 468 98 \times 10^3$ |
| 6.505 85 | $-0.511 478 27 \times 10^3$ | — | — | $-0.511 468 88 \times 10^3$ | — | $-0.511 467 95 \times 10^3$ | $-0.511 468 14 \times 10^3$ |
| 6.686 57 | $-0.511 477 87 \times 10^3$ | $-0.511 477 85 \times 10^3$ | $-0.511 477 99 \times 10^3$ | $-0.511 468 46 \times 10^3$ | $-0.511 468 53 \times 10^3$ | $-0.511 468 06 \times 10^3$ | $-0.511 467 73 \times 10^3$ |
| 6.867 28 | $-0.511 477 39 \times 10^3$ | $-0.511 477 54 \times 10^3$ | $-0.511 477 61 \times 10^3$ | $-0.511 467 98 \times 10^3$ | $-0.511 468 09 \times 10^3$ | $-0.511 467 90 \times 10^3$ | $-0.511 467 93 \times 10^3$ |
| 7.048 00 | $-0.511 476 84 \times 10^3$ | $-0.511 477 04 \times 10^3$ | $-0.511 477 12 \times 10^3$ | $-0.511 467 44 \times 10^3$ | $-0.511 467 59 \times 10^3$ | $-0.511 467 40 \times 10^3$ | $-0.511 467 43 \times 10^3$ |
| 7.228 72 | $-0.511 476 20 \times 10^3$ | $-0.511 476 40 \times 10^3$ | $-0.511 476 50 \times 10^3$ | $-0.511 466 80 \times 10^3$ | $-0.511 467 02 \times 10^3$ | $-0.511 466 79 \times 10^3$ | $-0.511 466 86 \times 10^3$ |

Table S4. Electronic transitions in CeF^{2+} and PaF^{3+} sorted by their absolute sensitivity Δq_1 to α variations as computed on the level of ZORA-cGHF.

| CeF^{2+} | | | | PaF^{3+} | | |
|-------------------|------------------------------------|-----------------------------|--|-------------------|------------------------------------|-----------------------------|
| Transition | $\Delta\tilde{\nu}/\text{cm}^{-1}$ | $\Delta q_1/\text{cm}^{-1}$ | | Transition | $\Delta\tilde{\nu}/\text{cm}^{-1}$ | $\Delta q_1/\text{cm}^{-1}$ |
| (3)3/2 ← (1)5/2 | 28 000 | −26 000 | | (3)3/2 ← (1)5/2 | 23 000 | −47 000 |
| (3)3/2 ← (2)3/2 | 28 000 | −26 000 | | (3)3/2 ← (1)7/2 | 24 000 | −46 000 |
| (3)3/2 ← (1)7/2 | 29 000 | −26 000 | | (3)3/2 ← (2)3/2 | 22 000 | −45 000 |
| (3)3/2 ← (2)1/2 | 27 000 | −26 000 | | (3)3/2 ← (1)3/2 | 28 000 | −43 000 |
| (3)3/2 ← (1)3/2 | 30 000 | −24 000 | | (3)3/2 ← (2)1/2 | 21 000 | −43 000 |
| (3)3/2 ← (X)5/2 | 31 000 | −24 000 | | (3)3/2 ← (X)5/2 | 30 000 | −42 000 |
| (3)3/2 ← (1)1/2 | 30 000 | −24 000 | | (3)3/2 ← (1)1/2 | 27 000 | −40 000 |
| (1)5/2 ← (1)1/2 | 1800 | 2400 | | (1)5/2 ← (1)1/2 | 3400 | 6600 |
| (2)3/2 ← (1)1/2 | 2300 | 2300 | | (1)7/2 ← (1)1/2 | 2500 | 5500 |
| (1)7/2 ← (1)1/2 | 850 | 2200 | | (2)3/2 ← (1)1/2 | 5000 | 4900 |
| (1)5/2 ← (X)5/2 | 3300 | 2200 | | (1)5/2 ← (X)5/2 | 6400 | 4700 |
| (2)3/2 ← (X)5/2 | 3800 | 2100 | | (2)1/2 ← (1)5/2 | 2400 | −3800 |
| (1)5/2 ← (1)3/2 | 2300 | 2100 | | (1)7/2 ← (X)5/2 | 5500 | 3600 |
| (1)7/2 ← (X)5/2 | 2300 | 2000 | | (1)5/2 ← (1)3/2 | 5200 | 3600 |
| (2)1/2 ← (1)1/2 | 2500 | 2000 | | (2)3/2 ← (X)5/2 | 8000 | 3000 |
| (2)3/2 ← (1)3/2 | 2700 | 2000 | | (1)1/2 ← (1)3/2 | 1800 | −3000 |
| (1)7/2 ← (1)3/2 | 1300 | 1900 | | (2)1/2 ← (1)1/2 | 5800 | 2800 |
| (2)1/2 ← (X)5/2 | 3900 | 1700 | | (2)1/2 ← (1)7/2 | 3300 | −2700 |
| (2)1/2 ← (1)3/2 | 2900 | 1600 | | (1)7/2 ← (1)3/2 | 4300 | 2600 |
| (2)1/2 ← (1)5/2 | 630 | −440 | | (2)1/2 ← (2)3/2 | 820 | −2100 |
| (1)1/2 ← (1)3/2 | 410 | −350 | | (2)3/2 ← (1)3/2 | 6800 | 2000 |
| (2)1/2 ← (2)3/2 | 160 | −330 | | (1)1/2 ← (X)5/2 | 3000 | −1900 |
| (2)1/2 ← (1)7/2 | 1600 | −280 | | (2)3/2 ← (1)5/2 | 1600 | −1700 |
| (1)1/2 ← (X)5/2 | 1500 | −220 | | (1)3/2 ← (X)5/2 | 1200 | 1100 |
| (1)5/2 ← (1)7/2 | 990 | 160 | | (1)5/2 ← (1)7/2 | 900 | 1100 |
| (1)3/2 ← (X)5/2 | 1000 | 120 | | (2)1/2 ← (X)5/2 | 8800 | 900 |
| (2)3/2 ← (1)5/2 | 460 | −110 | | (2)3/2 ← (1)7/2 | 2500 | −610 |
| (2)3/2 ← (1)7/2 | 1500 | 51 | | (2)1/2 ← (1)3/2 | 7600 | −180 |

Table S5. Values q_1 , $\langle H^{(2)} \rangle$, $\langle\langle H^{(1)}; H^{(1)} \rangle\rangle$ for individual electronic states at the respective equilibrium bond lengths of PaF^{3+} in the energetically lowest eight electronic states (at $c = c_0 = 137.0359895 a_0 E_h \hbar^{-1}$). As per equation (14) of the main text q_2 corresponds to the sum of an expectation value $\langle H^{(2)} \rangle$ and a response contribution $\langle\langle H^{(1)}; H^{(1)} \rangle\rangle$, here, with the Hamiltonians given in equation (24) and (25).

| State | $hc_0 q_1 / E_h$ | $\langle H^{(2)} \rangle / E_h$ | $\langle\langle H^{(1)}; H^{(1)} \rangle\rangle / E_h$ |
|--------|--|--|--|
| (X)5/2 | $-0.496\,949\,169\,591\,207 \times 10^4$ | $0.303\,180\,559\,063\,34 \times 10^4$ | $-0.693\,321\,864\,122\,968 \times 10^4$ |
| (1)3/2 | $-0.496\,948\,833\,200\,438 \times 10^4$ | $0.303\,180\,333\,762\,18 \times 10^4$ | $-0.693\,322\,288\,613\,604 \times 10^4$ |
| (1)1/2 | $-0.496\,950\,127\,145\,434 \times 10^4$ | $0.303\,180\,744\,242\,79 \times 10^4$ | $-0.693\,324\,494\,079\,290 \times 10^4$ |
| (1)7/2 | $-0.496\,947\,586\,927\,064 \times 10^4$ | $0.303\,181\,029\,027\,69 \times 10^4$ | $-0.693\,324\,571\,117\,269 \times 10^4$ |
| (1)5/2 | $-0.496\,947\,191\,574\,450 \times 10^4$ | $0.303\,180\,800\,098\,06 \times 10^4$ | $-0.693\,324\,677\,363\,224 \times 10^4$ |
| (2)3/2 | $-0.496\,947\,890\,869\,696 \times 10^4$ | $0.303\,180\,995\,412\,35 \times 10^4$ | $-0.693\,326\,520\,274\,510 \times 10^4$ |
| (2)1/2 | $-0.496\,948\,855\,155\,430 \times 10^4$ | $0.303\,181\,403\,111\,51 \times 10^4$ | $-0.693\,327\,072\,658\,838 \times 10^4$ |
| (3)3/2 | $-0.496\,968\,688\,624\,922 \times 10^4$ | $0.303\,188\,078\,871\,35 \times 10^4$ | $-0.693\,330\,099\,683\,591 \times 10^4$ |

Table S6. Values q_1 , $\langle H^{(2)} \rangle$, $\langle\langle H^{(1)}; H^{(1)} \rangle\rangle$ for individual electronic states at the respective equilibrium bond lengths of CeF^{2+} in the energetically lowest eight electronic states (at $c = c_0 = 137.0359895 a_0 E_h \hbar^{-1}$). As per equation (14) of the main text q_2 corresponds to the sum of an expectation value $\langle H^{(2)} \rangle$ and a response contribution $\langle\langle H^{(1)}; H^{(1)} \rangle\rangle$, here, with the Hamiltonians given in equation (24) and (25).

| State | $hc_0 q_1 / E_h$ | $\langle H^{(2)} \rangle / E_h$ | $\langle\langle H^{(1)}; H^{(1)} \rangle\rangle / E_h$ |
|--------|---------------------------|---------------------------------|--|
| (X)5/2 | $-511.474\,947\,005\,129$ | $67.312\,010\,500\,715\,4$ | $-258.195\,512\,678\,799$ |
| (1)3/2 | $-511.474\,385\,189\,328$ | $67.311\,907\,858\,284\,0$ | $-258.195\,451\,471\,348$ |
| (1)1/2 | $-511.475\,962\,842\,081$ | $67.312\,005\,891\,154\,7$ | $-258.196\,744\,264\,992$ |
| (1)7/2 | $-511.465\,728\,411\,338$ | $67.312\,169\,165\,077\,2$ | $-258.199\,141\,085\,717$ |
| (1)5/2 | $-511.464\,985\,708\,549$ | $67.312\,068\,658\,967\,9$ | $-258.198\,971\,946\,710$ |
| (2)3/2 | $-511.465\,477\,591\,613$ | $67.312\,092\,187\,750\,9$ | $-258.199\,627\,535\,626$ |
| (2)1/2 | $-511.466\,997\,502\,706$ | $67.312\,222\,689\,112\,3$ | $-258.200\,485\,072\,514$ |

Table S7. Total energies of CeF^{2+} as a function of the speed of light c , with $c_0 = 137.0359895 a_0 E_h h^{-1}$, calculated on the level of 2c-ZORA-cGFH with the internuclear distances for each electronic state reported in Tab. S1.

| $c/(a_0 E_h h^{-1})$ | (X)5/2 | (1)3/2 | (1)1/2 | E/E_h (1)7/2 | (1)5/2 | (2)3/2 | (2)1/2 |
|----------------------|---------------------|---------------------|---------------------|---------------------|---------------------|---------------------|---------------------|
| 123.035 989 5 | -9249.879 601 820 3 | -9249.874 710 432 3 | -9249.873 238 275 6 | -9249.866 982 915 6 | -9249.862 271 796 4 | -9249.860 296 630 7 | -9249.859 943 248 4 |
| 124.035 989 5 | -9239.092 691 125 3 | -9239.087 809 599 3 | -9239.086 299 542 0 | -9239.086 299 542 0 | -9239.075 543 213 2 | -9239.073 553 826 9 | -9239.073 166 641 3 |
| 125.035 989 5 | -9228.615 695 571 3 | -9228.610 823 843 9 | -9228.609 277 460 9 | -9228.603 409 744 0 | -9228.598 726 858 4 | -9228.596 724 093 6 | -9228.596 304 270 7 |
| 126.035 989 5 | -9218.436 349 863 2 | -9218.431 487 851 3 | -9218.429 906 594 2 | -9218.424 226 618 7 | -9218.419 557 458 3 | -9218.417 542 090 8 | -9218.417 090 727 8 |
| 127.035 989 5 | -9208.543 012 444 8 | -9208.538 160 053 1 | -9208.536 545 311 4 | -9208.531 049 177 4 | -9208.526 393 481 5 | -9208.524 366 219 3 | -9208.523 884 358 5 |
| 128.035 989 5 | -9198.924 626 580 7 | -9198.919 783 701 7 | -9198.918 136 769 1 | -9198.912 820 713 8 | -9198.908 178 220 5 | -9198.906 139 710 4 | -9198.905 628 342 0 |
| 129.035 989 5 | -9189.570 684 319 5 | -9189.565 850 835 6 | -9189.564 172 928 0 | -9189.559 033 307 1 | -9189.554 403 754 7 | -9189.552 354 587 8 | -9189.551 814 654 0 |
| 130.035 989 5 | -9180.471 193 092 6 | -9180.466 368 879 0 | -9180.464 661 141 5 | -9180.459 694 417 6 | -9180.455 077 547 7 | -9180.453 018 280 3 | -9180.452 450 663 0 |
| 131.035 989 5 | -9171.616 644 723 3 | -9171.611 829 647 5 | -9171.610 093 160 1 | -9171.605 295 903 7 | -9171.600 691 457 4 | -9171.598 622 577 5 | -9171.598 028 140 4 |
| 132.035 989 5 | -9162.997 986 647 5 | -9162.993 180 573 3 | -9162.991 146 353 9 | -9162.986 785 230 4 | -9162.982 192 956 0 | -9162.980 114 927 1 | -9162.979 494 476 6 |
| 133.035 989 5 | -9154.606 595 162 2 | -9154.601 797 947 4 | -9154.600 006 963 3 | -9154.595 538 734 3 | -9154.588 871 626 1 | -9154.588 225 931 3 | -9154.588 225 931 3 |
| 134.035 989 5 | -9146.434 250 535 9 | -9146.429 462 038 3 | -9146.427 645 193 2 | -9146.423 336 711 1 | -9146.418 768 027 8 | -9146.416 672 945 1 | -9146.416 002 742 9 |
| 135.035 989 5 | -9138.473 113 832 7 | -9138.468 333 903 8 | -9138.466 492 064 1 | -9138.462 340 263 7 | -9138.457 783 011 0 | -9138.455 679 956 3 | -9138.454 985 951 6 |
| 136.035 989 5 | -9130.715 703 312 0 | -9130.710 933 806 5 | -9130.709 067 789 7 | -9130.705 069 689 5 | -9130.700 523 625 7 | -9130.698 412 944 6 | -9130.697 695 795 0 |
| 136.635 989 5 | -9126.156 065 666 9 | -9126.151 299 143 8 | -9126.149 418 993 4 | -9126.145 511 714 4 | -9126.140 972 253 8 | -9126.138 857 133 4 | -9126.138 126 421 2 |
| 136.735 989 5 | -9125.402 900 725 1 | -9125.398 135 021 8 | -9125.396 252 548 5 | -9125.392 360 307 4 | -9125.387 821 937 2 | -9125.385 706 085 9 | -9125.384 973 136 6 |
| 136.835 989 5 | -9124.651 653 335 9 | -9124.646 888 462 2 | -9124.645 003 654 5 | -9124.641 126 428 0 | -9124.636 589 148 0 | -9124.634 472 579 9 | -9124.633 373 388 6 |
| 136.935 989 5 | -9123.902 316 757 9 | -9123.897 552 706 1 | -9123.895 665 590 2 | -9123.891 803 337 4 | -9123.887 267 145 4 | -9123.885 149 847 3 | -9123.884 412 436 4 |
| 137.035 989 5 | -9123.154 884 280 7 | -9123.150 121 049 7 | -9123.148 231 631 3 | -9123.144 384 326 0 | -9123.139 849 219 0 | -9123.137 731 207 5 | -9123.136 991 569 2 |
| 137.135 989 5 | -9122.409 349 224 5 | -9122.404 586 813 7 | -9122.402 695 086 1 | -9122.398 862 712 3 | -9122.394 328 688 6 | -9122.392 209 964 7 | -9122.391 468 107 0 |
| 137.235 989 5 | -9121.665 704 939 0 | -9121.660 943 344 5 | -9121.659 049 321 9 | -9121.655 231 849 0 | -9121.650 698 905 8 | -9121.648 579 461 2 | -9121.647 835 400 1 |
| 137.335 989 5 | -9120.923 944 804 9 | -9120.919 184 027 1 | -9120.917 287 723 6 | -9120.913 485 112 6 | -9120.908 953 246 8 | -9120.906 833 091 5 | -9120.906 086 828 8 |
| 137.435 989 5 | -9120.184 062 232 3 | -9120.179 302 268 4 | -9120.177 403 697 9 | -9120.173 615 915 7 | -9120.169 085 126 2 | -9120.166 964 260 9 | -9120.166 215 803 2 |
| 138.035 989 5 | -9115.783 830 285 2 | -9115.779 075 178 1 | -9115.777 163 096 9 | -9115.773 463 760 2 | -9115.768 939 377 3 | -9115.766 814 330 6 | -9115.766 052 807 6 |
| 139.035 989 5 | -9108.596 025 539 3 | -9108.591 278 408 8 | -9108.589 344 364 5 | -9108.585 790 238 4 | -9108.581 276 354 9 | -9108.579 144 528 2 | -9108.578 361 718 0 |
| 140.035 989 5 | -9101.585 238 494 1 | -9101.580 499 192 9 | -9101.578 543 860 1 | -9101.575 132 250 0 | -9101.570 628 644 0 | -9101.568 490 291 7 | -9101.567 686 748 5 |
| 141.035 989 5 | -9094.745 508 466 1 | -9094.740 776 844 2 | -9094.738 800 853 1 | -9094.735 529 147 4 | -9094.731 035 601 4 | -9094.728 890 952 1 | -9094.728 067 215 1 |
| 142.035 989 5 | -9088.071 131 241 7 | -9088.066 407 157 1 | -9088.064 411 115 3 | -9088.061 276 749 9 | -9088.056 793 053 8 | -9088.054 642 323 4 | -9088.053 798 906 6 |
| 143.035 989 5 | -9081.556 645 587 8 | -9081.551 928 893 7 | -9081.549 913 383 8 | -9081.546 913 865 8 | -9081.542 439 808 4 | -9081.540 283 197 3 | -9081.539 420 594 3 |
| 144.035 989 5 | -9075.196 820 603 4 | -9075.192 111 155 9 | -9075.190 076 730 1 | -9075.187 209 626 1 | -9075.182 745 004 8 | -9075.180 582 695 2 | -9075.179 701 384 1 |
| 145.035 989 5 | -9068.986 643 850 6 | -9068.981 941 510 7 | -9068.979 888 700 2 | -9068.977 151 629 1 | -9068.972 696 244 4 | -9068.970 528 413 3 | -9068.969 628 847 1 |
| 146.035 989 5 | -9062.921 310 208 9 | -9062.916 614 835 9 | -9062.914 544 148 9 | -9062.911 934 786 1 | -9062.907 488 446 0 | -9062.905 315 253 4 | -9062.904 397 871 7 |
| 147.035 989 5 | -9056.996 211 403 3 | -9056.991 522 862 2 | -9056.989 434 780 2 | -9056.986 950 856 7 | -9056.982 513 374 0 | -9056.980 334 972 3 | -9056.979 200 196 1 |
| 148.035 989 5 | -9051.206 926 158 2 | -9051.202 244 313 4 | -9051.200 139 300 1 | -9051.197 778 605 4 | -9051.193 349 791 7 | -9051.191 166 323 7 | -9051.190 214 555 3 |
| 149.035 989 5 | -9045.549 210 933 9 | -9045.544 535 652 3 | -9045.542 414 158 5 | -9045.540 174 525 5 | -9045.535 754 196 0 | -9045.533 565 795 0 | -9045.532 597 425 9 |
| 150.035 989 5 | -9040.018 991 206 6 | -9040.014 322 358 3 | -9040.012 184 808 1 | -9040.010 064 122 8 | -9040.005 652 102 3 | -9040.003 458 893 2 | -9040.002 474 297 3 |
| 151.035 989 5 | -9034.612 353 252 8 | -9034.607 690 710 6 | -9034.605 537 517 4 | -9034.603 533 705 9 | -9034.599 129 825 6 | -9034.596 931 923 9 | -9034.595 931 462 8 |

Table S8. Total energies of CeF^{2+} as a function of the speed of light c , with $c_0 = 137.0359895 a_0 E_h h^{-1}$, calculated on the level of AOC-DHF with the internuclear distances for each electronic state reported in Tab. S1.

| $c/(a_0 E_h h^{-1})$ | (X)5/2 | (1)3/2 | (1)1/2 | E/E_h (1)7/2 | (1)5/2 | (2)3/2 | (2)1/2 |
|----------------------|-------------------------|-------------------------|-------------------------|-------------------------|-------------------------|-------------------------|-------------------------|
| 123.035 989 5 | -9040.342 303 358 349 5 | -9040.336 622 546 132 3 | -9040.334 126 844 647 5 | -9040.330 665 284 827 8 | -9040.325 409 298 728 1 | -9040.322 884 110 812 1 | -9040.321 462 946 989 4 |
| 124.035 989 5 | -9033.583 074 813 033 8 | -9033.577 404 401 336 0 | -9033.574 869 999 583 8 | -9033.571 591 487 805 6 | -9033.566 349 320 786 7 | -9033.563 810 811 352 6 | -9033.562 351 710 381 3 |
| 125.035 989 5 | -9027.012 527 705 084 7 | -9027.006 867 626 119 9 | -9027.004 296 234 683 4 | -9027.001 196 689 054 3 | -9026.995 968 089 402 6 | -9026.993 417 073 796 1 | -9026.991 921 307 508 2 |
| 126.035 989 5 | -9020.623 433 355 234 7 | -9020.617 783 526 116 9 | -9020.615 176 750 674 4 | -9020.612 252 229 037 0 | -9020.607 036 943 607 5 | -9020.604 474 167 323 1 | -9020.602 942 940 229 7 |
| 127.035 989 5 | -9014.408 918 360 501 0 | -9014.403 278 687 850 6 | -9014.400 638 037 617 7 | -9014.397 884 728 876 3 | -9014.392 682 503 938 0 | -9014.390 108 649 238 8 | -9014.388 543 103 667 0 |
| 128.035 989 5 | -9008.362 443 170 894 0 | -9008.356 813 550 946 8 | -9008.354 140 447 450 8 | -9008.351 554 662 705 9 | -9008.346 365 245 335 6 | -9008.344 780 938 288 5 | -9008.342 182 158 601 6 |
| 129.035 989 5 | -9002.477 782 198 391 7 | -9002.472 162 519 274 2 | -9002.469 458 303 019 6 | -9002.467 036 469 204 7 | -9002.461 859 607 670 7 | -9002.459 265 422 237 9 | -9002.457 634 439 240 8 |
| 130.035 989 5 | -8996.749 095 333 577 8 | -8996.743 395 477 178 6 | -8996.740 661 413 759 9 | -8996.738 006 046 406 0 | -8996.733 235 510 941 1 | -8996.730 331 976 492 1 | -8996.728 969 769 934 3 |
| 131.035 989 5 | -8991.170 460 755 445 7 | -8991.164 860 599 037 6 | -8991.162 097 885 398 9 | -8991.159 993 662 679 0 | -8991.154 841 165 796 8 | -8991.152 228 768 465 6 | -8991.150 536 271 337 8 |
| 132.035 989 5 | -8985.736 758 928 665 9 | -8985.731 168 345 182 6 | -8985.728 378 114 849 0 | -8985.726 427 752 431 8 | -8985.721 287 070 369 7 | -8985.718 666 258 841 0 | -8985.716 944 360 026 9 |
| 133.035 989 5 | -8980.442 757 693 821 5 | -8980.437 176 553 092 3 | -8980.434 359 880 289 8 | -8980.432 560 206 498 2 | -8980.427 431 097 739 8 | -8980.424 802 286 561 3 | -8980.423 051 833 662 6 |
| 134.035 989 5 | -8975.283 548 361 239 8 | -8975.277 976 531 593 6 | -8975.275 314 435 756 6 | -8975.273 482 367 185 4 | -8975.268 364 595 174 7 | -8975.265 728 166 941 7 | -8975.263 949 969 255 9 |
| 135.035 989 5 | -8970.254 442 736 215 4 | -8970.248 880 083 852 8 | -8970.246 013 534 839 2 | -8970.244 506 070 632 3 | -8970.239 399 402 040 4 | -8970.236 755 711 770 5 | -8970.234 950 540 238 1 |
| 136.035 989 5 | -8965.350 960 995 450 8 | -8965.345 407 386 688 7 | -8965.342 517 306 420 6 | -8965.341 151 526 900 9 | -8965.336 055 733 132 5 | -8965.333 405 109 484 4 | -8965.331 573 703 211 7 |
| 136.635 989 5 | -8962.467 381 904 114 5 | -8962.461 833 657 218 4 | -8962.458 929 882 494 0 | -8962.457 647 745 432 0 | -8962.452 558 366 838 3 | -8962.449 903 730 726 9 | -8962.448 056 924 355 1 |
| 136.735 989 5 | -8961.990 968 964 930 3 | -8961.985 421 607 219 9 | -8961.982 515 580 404 7 | -8961.981 247 284 536 9 | -8961.976 158 967 729 1 | -8961.973 503 673 611 0 | -8961.971 654 324 534 0 |
| 136.835 989 5 | -8961.515 740 424 611 1 | -8961.510 193 954 760 3 | -8961.507 285 683 464 9 | -8961.506 031 202 267 0 | -8961.500 943 944 554 8 | -8961.498 287 994 754 7 | -8961.496 436 110 177 5 |
| 136.935 989 5 | -8961.041 692 233 540 7 | -8961.036 146 649 132 2 | -8961.033 236 142 806 3 | -8961.031 995 448 001 9 | -8961.026 909 247 128 1 | -8961.024 252 645 214 8 | -8961.022 398 231 538 3 |
| 137.035 989 5 | -8960.568 820 358 472 3 | -8960.563 275 659 489 6 | -8960.560 362 926 336 9 | -8960.559 135 989 244 2 | -8960.554 050 843 884 4 | -8960.551 391 501 642 4 | -8960.549 536 656 404 6 |
| 137.135 989 5 | -8960.097 120 786 307 6 | -8960.091 576 970 453 4 | -8960.088 662 018 832 1 | -8960.087 448 812 005 3 | -8960.082 364 719 637 6 | -8960.079 706 820 290 1 | -8960.077 847 370 073 9 |
| 137.235 989 5 | -8959.626 589 518 657 1 | -8959.621 046 585 602 0 | -8959.618 129 423 204 7 | -8959.616 929 919 628 1 | -8959.611 846 877 325 7 | -8959.609 188 334 196 0 | -8959.607 326 374 820 3 |
| 137.335 989 5 | -8959.157 222 576 968 7 | -8959.151 680 524 339 1 | -8959.148 761 160 440 7 | -8959.147 575 332 786 8 | -8959.142 493 338 673 4 | -8959.139 834 154 293 6 | -8959.137 969 693 289 1 |
| 137.435 989 5 | -8958.689 015 999 450 9 | -8958.683 474 826 231 8 | -8958.680 553 268 906 8 | -8958.679 381 089 017 6 | -8958.674 300 140 908 6 | -8958.671 640 317 950 7 | -8958.669 773 361 703 8 |
| 138.035 989 5 | -8955.903 924 487 052 8 | -8955.898 388 563 380 6 | -8955.895 454 014 435 | | | | |

Table S9. Total energies of CeF^{2+} as a function of the speed of light c , with $c_0 = 137.0359895 a_0 E_h \hbar^{-1}$, calculated on the level of AOC-DHF-FSCSD with the internuclear distances for each electronic state set to $r = 3.5392944488 a_0$.

| $c/(a_0 E_h \hbar^{-1})$ | (X)5/2 | (1)3/2 | (1)1/2 | E/E_h (1)7/2 | (1)5/2 | (2)3/2 | (2)1/2 |
|--------------------------|--------------------|--------------------|--------------------|--------------------|--------------------|--------------------|--------------------|
| 125.0359895 | -9028.151955150770 | -9028.149984892745 | -9028.146073649370 | -9028.140190409373 | -9028.139212289434 | -9028.135307322404 | -9028.133774166785 |
| 127.0359895 | -9015.547829250103 | -9015.545880203093 | -9015.541879081566 | -9015.536369438474 | -9015.535416943314 | -9015.531437045414 | -9015.529871043738 |
| 129.0359895 | -9003.616189976461 | -9003.614262644945 | -9003.610180400170 | -9003.605025160936 | -9003.604097373001 | -9003.600048257205 | -9003.598455499407 |
| 131.0359895 | -8992.308378280259 | -8992.306472932687 | -8992.302317323702 | -8992.297498795022 | -8992.296594762449 | -8992.292481321383 | -8992.290867475960 |
| 133.0359895 | -8981.580197307636 | -8981.578314035409 | -8981.574091954695 | -8981.569593766424 | -8981.568712527940 | -8981.564538968089 | -8981.562909307240 |
| 135.0359895 | -8971.391416327288 | -8971.389555089378 | -8971.385272672980 | -8971.381079630648 | -8971.380220232888 | -8971.375990184144 | -8971.374349607568 |
| 137.0359895 | -8961.705339402562 | -8961.703500059388 | -8961.699162781169 | -8961.695260741553 | -8961.694422250799 | -8961.690138856444 | -8961.688491913626 |
| 140.0359895 | -8948.046212908133 | -8948.044405992096 | -8948.039995432337 | -8948.036505420734 | -8948.035696601446 | -8948.031338197454 | -8948.029689520481 |
| 143.0359895 | -8935.341816891256 | -8935.340041763646 | -8935.335567269574 | -8935.332462387509 | -8935.331681314081 | -8935.327252917126 | -8935.325610975133 |
| 146.0359895 | -8923.502824696099 | -8923.501080621339 | -8923.496550149617 | -8923.493805940854 | -8923.493050811632 | -8923.488556536349 | -8923.486928856701 |
| 149.0359895 | -8912.450373763002 | -8912.448659955322 | -8912.444080305491 | -8912.441674446627 | -8912.440943586882 | -8912.436386831283 | -8912.434780079955 |
| 152.0359895 | -8902.114595898040 | -8902.112911552884 | -8902.108288559182 | -8902.106200601176 | -8902.105492460731 | -8902.100876050934 | -8902.099296105351 |